AD-A037 665 TEL-AVIV UNIV (ISRAEL) DEPT OF MATHEMATICAL SCIENCES F/G 20/4
THE NUMERICAL COMPUTATIONS OF SUPERSONIC FLOW PAST BLUNT BODIES--ETC(U)
1976 S S ABARBANEL AF-AFOSR-2370-72
UNCLASSIFIED AFOSR-TR-77-0162 NL

1 OF 1
ADA037665

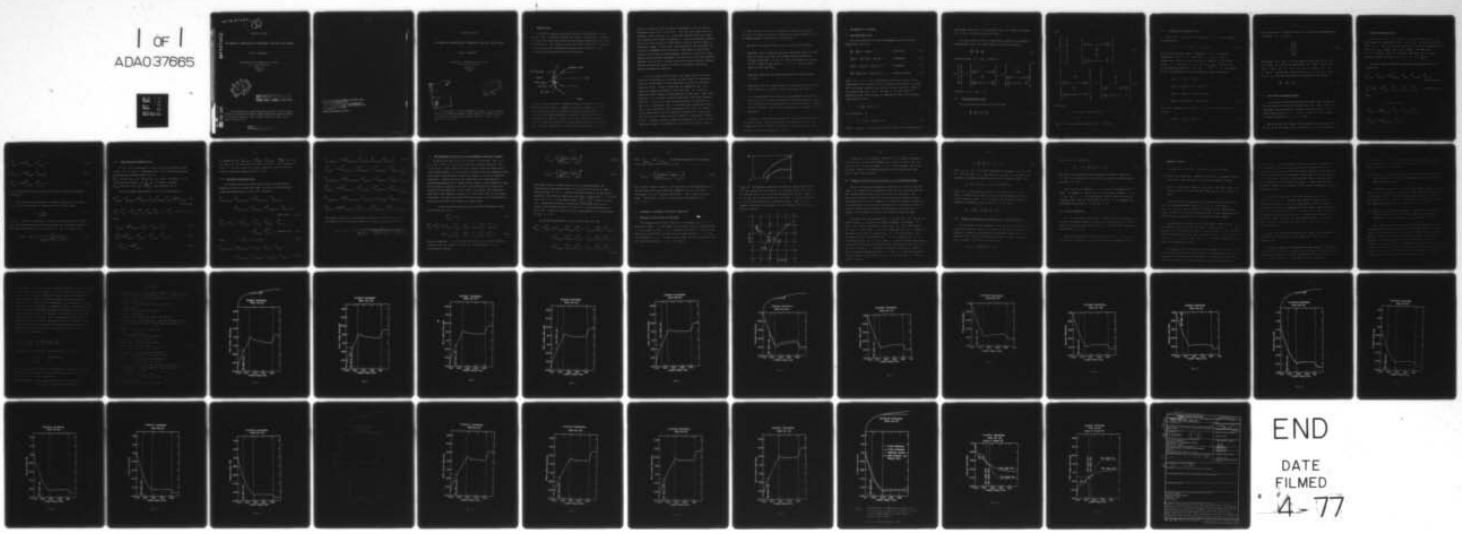

END
DATE FILMED
4-77

TECHNICAL REPORT

THE NUMERICAL COMPUTATIONS OF SUPERSONIC FLOW PAST BLUNT BODIES

SAUL S. ABARBANEL

Department of Mathematical Sciences
Tel Aviv University
Ramat Aviv
ISRAEL

THIS RESEARCH HAS BEEN SPONSORED IN PART BY THE AIR FORCE OFFICE OF SCIENTIFIC RESEARCH (NAM) THROUGH THE EUROPEAN OFFICE OF AEROSPACE RESEARCH, AFSC, UNITED STATES AIR FORCE, UNDER GRANT AFOSR-72-2370.

AIR FORCE OFFICE OF SCIENTIFIC RESEARCH (AFSC)
NOTICE OF TRANSMITTAL TO DDC
This technical report has been reviewed and is
approved for public release IAW AFR 190-12 (7b).
Distribution is unlimited.
A. D. BLOSE
Technical Information Officer

TECHNICAL REPORT

THE NUMERICAL COMPUTATIONS OF SUPERSONIC FLOW PAST BLUNT BODIES

SAUL S. ABARBANEL

Department of Mathematical Sciences
Tel Aviv University
Ramat Aviv
ISRAEL

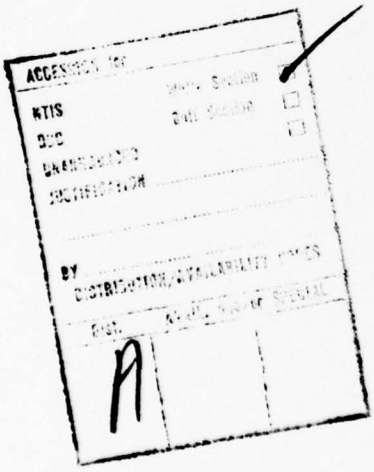

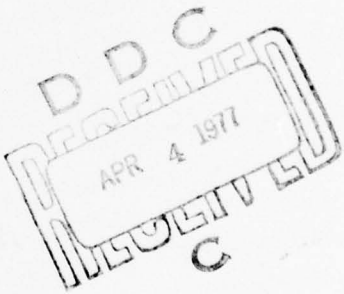

THIS RESEARCH HAS BEEN SPONSORED IN PART BY THE AIR FORCE OFFICE OF SCIENTIFIC RESEARCH (NAM) THROUGH THE EUROPEAN OFFICE OF AEROSPACE RESEARCH, AFSC, UNITED STATES AIR FORCE, UNDER GRANT AFOSR-72-2370.

1. INTRODUCTION

Solving the equations governing inviscid fluid mechanics is not an easy task - essentially because the system is non-linear. In addition, in steady flow past blunt bodies various regions differ from each other mathematically - the subsonic flow at the front of the body is governed by elliptic partial differential equations while the same set of equations become hyperbolic farther downstream.

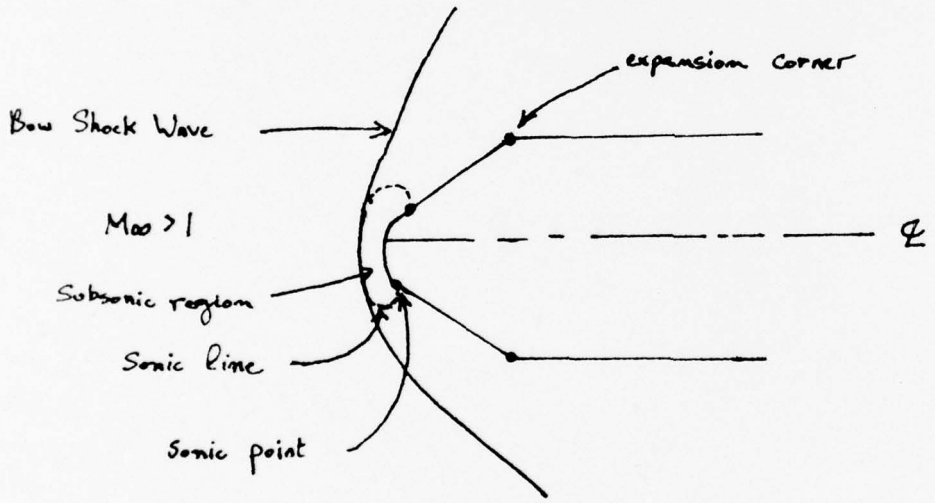

Fig. 1

Because of the difficulty in obtaining analytic solutions there were developed, in the 1950's, a number of numerical methods. Two of the better known ones were the method of Integral Relations due to Dorodnitsyn and Belotserkovskii [1] and the Inverse Body Method of Garabedian [2]. Both are usually used in the subsonic region only with the method of characteristics being employed for the supersonic flow. These two algorithms are efficient from the point of view of

speed of calculation and core memory requirements. They do, however, encounter difficulties in two areas: near the sonic point and at the expansion corner (see Fig. 1). Since these methods solve the steady flow equations they cannot be applied to truly time dependent problems - such as the diffraction of a shock wave by the bow wave of a body in supersonic flight. In the 1960's Lax and Wendroff [3], Richtmyer [4] and others developed finite-differences algorithms of second order accuracy for solving the time dependent equations. In principle these methods possess several advantages: the ability to treat time dependent problems, the ability to include shock waves without special treatment and the fact that the whole flow field is governed by hyperbolic partial differential equations.

It is also found that the sonic line region and the expansion corner do not present any difficulty to these types of computations. The major disadvantage of these algorithms is having an additional dimension (time) - thereby increasing the computation time. The length of computation depends on the time step, Δt, which the algorithm allows without causing numerical instabilities. Thus, where possible, it is desirable to devise algorithms with larger allowable time step. Zwas [5] has modified the Richtmyer two step method so that Δt is increased by 40% in two-dimensional calculations and by 70% in three dimensions. Flows containing shock waves are subject to little understood *non-linear* numerical instabilities. Harten and Zwas [6] show how to deal with this problem by employing the Shuman filter. Goldberg, Gottlieb, Turkel and Abarbanel [7], [8], [9], [10], developed a number of algorithms for achieving high order accuracy

(4th order and more) and also considered the theoretical problems connected with applying boundary conditions at moving boundaries (e.g. the Rankin-Hugoniot conditions at a shock wave).

The specific problems solved in this report are as follows:

1. Supersonic flow of ideal gas past two dimensional bodies at zero angle of attack. The bodies are blunted wedges connected to straight afterbodies (see Fig. 1). The calculations were carried out for a range of Mach numbers, $2 \leq M \leq 4$, and for various values of the wedge angle.

2. Supersonic flow past two dimensional bodies at various angles of attack.

3. Supersonic flow past blunted bodies of revolution such as blunted cone followed by a circular cylinder afterbody (see Fig. 1).

4. A 3-D calculation of the flow past an axisymmetric body. While this *problem* is not truly axisymmetric the calculation was carried in 3-D and the results compared well with the axisymmetric computations for the same body. [These results encourage us to attempt truly 3-D problems.]

In Section 2 are presented the partial differential equations for the various cases; Section 3 describes the numerical scheme; the boundary and initial conditions treatment is given in Section 4 and Section 5 discusses the numerical results.

2. THE EQUATIONS OF MOTION

(i) Two Dimensional Flow

The Euler equations for the time dependent flow of inviscid, compressible fluid are:

$$\frac{\partial \rho}{\partial t} + \frac{\partial}{\partial x}(\rho u) + \frac{\partial}{\partial y}(\rho v) = 0 \qquad \text{(Continuity)} \qquad (2.1)$$

$$\frac{\partial}{\partial t}(\rho u) + \frac{\partial}{\partial x}(\rho u^2+p) + \frac{\partial}{\partial y}(\rho uv) = 0 \qquad \text{(x-momentum)} \qquad (2.2)$$

$$\frac{\partial}{\partial t}(\rho v) + \frac{\partial}{\partial x}(\rho vu) + \frac{\partial}{\partial y}(\rho v^2+p) = 0 \qquad \text{(y-momentum)} \qquad (2.3)$$

$$\frac{\partial E}{\partial t} + \frac{\partial}{\partial x}[u(E+p)] + \frac{\partial}{\partial y}[v(E+p)] = 0 \qquad \text{(Energy equation)} \qquad (2.4)$$

where u, v, ρ, p, E are, respectively, the fluid velocity in the x-direction, fluid velocity in the y-direction, the density, pressure and *total* energy (internal plus kinetic energies) per unit volume of the fluid at the point (x, y) at time t. We still have to characterize the fluid through its equation of state. We'll consider ideal gases for which

$$E = \frac{p}{\gamma-1} + \frac{1}{2}\rho(u^2+ v^2) \qquad (2.5)$$

or, solving for p,

$$p = (\gamma-1)[E - \frac{1}{2}\rho(u^2+ v^2)] \qquad (2.6)$$

where $\gamma = c_p/c_v$ is the ratio of specific heats at constant pressure

and volume respectively. For hypersonic flow, for example, one would have to use a different equation of state.

The above system of partial differential equations is written in divergenceless form. In vector notation it may be written as

$$\frac{\partial W}{\partial t} = \frac{\partial F}{\partial x} + \frac{\partial G}{\partial y} \tag{2.7}$$

with the vectors W, F and G given by

(2.8)

$$W = \begin{bmatrix} \rho \\ m \\ n \\ E \end{bmatrix} ; \quad F = \begin{bmatrix} - m \\ \frac{(\gamma-3)}{2\rho} m^2 - (\gamma-1)(E-\frac{n^2}{2\rho}) \\ - \frac{mn}{\rho} \\ \frac{(\gamma-1)}{2\rho^2} m(m^2+n^2) - \frac{\gamma E m}{\rho} \end{bmatrix} ; \quad G = \begin{bmatrix} - n \\ - \frac{nm}{\rho} \\ \frac{(\gamma-3)}{2\rho} n^2 - (\gamma-1)(E-\frac{m^2}{2\rho}) \\ \frac{(\gamma-1)}{2\rho^2} n(m^2+n^2) - \frac{\gamma E n}{\rho} \end{bmatrix}$$

and where $m = \rho u$ and $n = \rho v$.

(ii) Three Dimensional Flow

The conservation equations are of the form:

$$\frac{\partial W}{\partial t} = \frac{\partial F}{\partial x} + \frac{\partial G}{\partial y} + \frac{\partial H}{\partial z} \tag{2.9}$$

where

$$W = \begin{bmatrix} \rho \\ m \\ n \\ \ell \\ E \end{bmatrix} ; \qquad F = \begin{bmatrix} - m \\ \frac{(\gamma-3)}{2\rho} m^2 - (\gamma-1)(E - \frac{n^2+\ell^2}{2\rho}) \\ - \frac{mn}{\rho} \\ - \frac{m\ell}{\rho} \\ \frac{(\gamma-1)}{2\rho^2} m(m^2+n^2+\ell^2) - \frac{\gamma m E}{\rho} \end{bmatrix} \tag{2.10}$$

$$G = \begin{bmatrix} - n \\ - \frac{mn}{\rho} \\ \frac{(\gamma-3)}{2\rho} n^2 - (\gamma-1)(E - \frac{m^2+\ell^2}{2\rho}) \\ - \frac{n\ell}{\rho} \\ \frac{(\gamma-1)}{2\rho^2} n(m^2+n^2+\ell^2) - \frac{\gamma n E}{\rho} \end{bmatrix} ; \qquad H = \begin{bmatrix} - \ell \\ - \frac{m\ell}{\rho} \\ - \frac{n\ell}{\rho} \\ \frac{(\gamma-3)}{2\rho} \ell^2 - (\gamma-1)(E - \frac{m^2+n^2}{2\rho}) \\ \frac{(\gamma-1)}{2\rho^2} \ell(m^2+n^2+\ell^2) - \frac{\gamma \ell E}{\rho} \end{bmatrix} \tag{2.11}$$

where now

$$p = (\gamma-1)[E - \tfrac{1}{2}\rho(u^2+v^2+w^2)] \tag{2.12}$$

$$\ell = \rho w \tag{2.13}$$

and w is the velocity component in the z direction.

(iii) Cylindrically Symmetric Flow

We get this case from the 3-D equations (2.9) - (2.13) through the substitution

$$x = x, \qquad y = r \sin\theta, \qquad z = r \cos\theta, \tag{2.14}$$

and by going from the velocity components u, v, w to velocity components in the x, r, θ directions - i.e. u_x, u_r and u_θ respectively. Since we assume cylindrical symmetry, we may as well assume $u_\theta = 0$ and label u_x and u_r by u and v respectively. All variables now depend on t, x and $r = \sqrt{y^2 + z^2}$. As a consequence of this transformation we get the following system of equations:

$$\frac{\partial}{\partial t}(r\rho) + \frac{\partial}{\partial x}(r\rho u) + \frac{\partial}{\partial r}(r\rho v) = 0 \tag{2.15}$$

$$\frac{\partial}{\partial t}(r\rho u) + \frac{\partial}{\partial x}[r(\rho u^2+p)] + \frac{\partial}{\partial r}(r\rho uv) = 0 \tag{2.16}$$

$$\frac{\partial}{\partial t}(r\rho v) + \frac{\partial}{\partial x}(r\rho vu) + \frac{\partial}{\partial r}[r(\rho v^2+p)] = p \tag{2.17}$$

$$\frac{\partial}{\partial t}(rE) + \frac{\partial}{\partial x}[ru(E+p)] + \frac{\partial}{\partial r}[rv(E+p)] = 0 \quad . \tag{2.18}$$

Notice the inhomogeneous term in Eq. (2.17). The vector form of this system is

$$\frac{\partial}{\partial t}(rW) = \frac{\partial}{\partial x}(rF) + \frac{\partial}{\partial r}(rG) + S \tag{2.19}$$

where the pressure is again defined as in (2.6) and the nonhomogeneous term vector, S, is given by

$$S = \begin{pmatrix} 0 \\ 0 \\ p \\ 0 \end{pmatrix} \quad . \tag{2.20}$$

The vectors W, F and G are the same as those given in Eq. (2.8). If we label $W' \equiv rW$ we see immediately that $rF(W) = F(W')$ and $rG(w) = G(W')$. Let $F' \equiv F(W') = rF$ and $G' \equiv G(W') = rG$; i.e. F' and G' are the same vector functions of $W' = rW$ as F and G were of W. Thus our task becomes the solution of the system

$$\frac{\partial W'}{\partial t} = \frac{\partial F'}{\partial x} + \frac{\partial G'}{\partial r} + S \quad . \tag{2.21}$$

3. THE FINITE DIFFERENCE SCHEMES

In all cases described herein the algorithms used are based on a two step scheme à la Zwas and Burstein [5], [11], [12]. In the two-dimensional and cylindrically symmetric cases the schemes use 9 computational points in a 3×3 net. In the 3-D case we require 27 points constituting a $3 \times 3 \times 3$ cube.

We now present the schemes, their linear stability criteria and the way we use the Shuman filter to prevent *non-linear* instabilities.

(i) The Two-Dimensional Case

The vectors $W(x, y, t)$, $F(W(x, y, t))$ and $G(W(x, y, t,))$ are approximated by discretized vectors. Thus $W^n_{j,k} = W(j\Delta x, k\Delta y, t_n) = W(x,y,t)$ where Δx, Δy and Δt_n are the step sizes in the finite difference net. Similarly $F^n_{j,k} = F(W^n_{j,k})$ and $G^n_{j,k} = G(W^n_{j,k})$. We shall take $\Delta y = \Delta x =$ constant, but Δt_n may vary. The number of time steps required to reach the time t_n is n ; i.e. $t_n = \sum_{m=1}^{n} \Delta t_m$.

The basic finite difference scheme approximating the system (2.7) is given by:

$$W^{n+\frac{1}{2}}_{j+\frac{1}{2},k+\frac{1}{2}} = \hat{W}^n_{j+\frac{1}{2},k+\frac{1}{2}} + \frac{\lambda}{2}[\tilde{F}^n_{j+1,k+\frac{1}{2}} - \tilde{F}^n_{j,k+\frac{1}{2}} + \tilde{G}^n_{j+\frac{1}{2},k+1} - \tilde{G}^n_{j+\frac{1}{2},k}] \quad \text{(first step)} \quad (3.1)$$

$$W^{n+1}_{j,k} = W^n_{j,k} + \lambda[\tilde{F}^{n+\frac{1}{2}}_{j+\frac{1}{2},k} - \tilde{F}^{n+\frac{1}{2}}_{j-\frac{1}{2},k} + \tilde{G}^{n+\frac{1}{2}}_{j,k+\frac{1}{2}} - \tilde{G}^{n+\frac{1}{2}}_{j,k-\frac{1}{2}}] \quad \text{(second step)} \quad (3.2)$$

where

$$\lambda = \Delta t/\Delta x = \Delta t/\Delta y \quad (3.3)$$

$$\hat{W}^n_{j+\frac{1}{2},k+\frac{1}{2}} = \frac{1}{4}[W^n_{j+1,k+1} + W^n_{j+1,k} + W^n_{j,k+1} + W^n_{j,k}] \quad (3.4)$$

$$\tilde{F}^n_{j+1,k+\frac{1}{2}} = F(\frac{1}{2}(W^n_{j+1,k+1} + W^n_{j+1,k})) \quad (3.5)$$

$$\underset{\sim}{F}^{n+\frac{1}{2}}_{j+\frac{1}{2},k} = F\left(\frac{1}{2}\left(W^{n+\frac{1}{2}}_{j+\frac{1}{2},k+\frac{1}{2}} + W^{n+\frac{1}{2}}_{j+\frac{1}{2},k-\frac{1}{2}}\right)\right) \tag{3.6}$$

$$\underset{\sim}{G}^{n}_{j+\frac{1}{2},k+1} = G\left(\frac{1}{2}\left(W^{n}_{j,k+1} + W^{n}_{j+1,k+1}\right)\right) \tag{3.7}$$

$$\underset{\sim}{G}^{n+\frac{1}{2}}_{j,k+\frac{1}{2}} = G\left(\frac{1}{2}\left(W^{n+\frac{1}{2}}_{j+\frac{1}{2},k+\frac{1}{2}} + W^{n+\frac{1}{2}}_{j-\frac{1}{2},k+\frac{1}{2}}\right)\right) \quad , \tag{3.8}$$

with similar expressions holding for discrete vectors with different subscripts.

The criterion for the numerical (linear) stability of the scheme (3.1) + (3.2) constrains the time step to be (see Ref. [11]):

$$\Delta t \leq \frac{\Delta x}{c+\sqrt{u^2+v^2}} \tag{3.9}$$

where $c = (\gamma p/\rho)^{\frac{1}{2}}$ is the speed of sound. In practice, one has to check all the involved qualities at each grid point and select the minimum of the right hand side of Eq. (3.9) over all j and k. Thus, we use

$$\Delta t_{n+1} = t_{n+1} - t_n \leq \frac{\Delta x}{\max\limits_{j,k}\left[c^n_{j,k}+\sqrt{(u^n_{j,k})^2+(v^n_{j,k})^2}\right]} \tag{3.10}$$

(ii) The Cylindrical Symmetry Case

For the sake of convenience we shall drop now the primes of the vectors W', F' and G' appearing in Eq. (2.21) and the discretized approximations of these vectors will be

$W^n_{j,k} = W'(j\Delta x, k\Delta r, t_n) = rW(j\Delta x, k\Delta r, t_n)$ where, as before $\Delta x = \Delta r$ is the grid size while $t_n = \sum_{m=1}^{n} \Delta t_m$. As before, we define $F^n_{j,k} = F(W'(j\Delta x, k\Delta r, t_n)) = F(W^n_{j,k})$ and similarly for G'.

The basic scheme representing Eq. (2.21) is given then by:

$$W^{n+\frac{1}{2}}_{j+\frac{1}{2},k+\frac{1}{2}} = \hat{W}^{n}_{j+\frac{1}{2},k+\frac{1}{2}} + \frac{\lambda}{2}[\tilde{F}^{n}_{j+1,k+\frac{1}{2}} - \tilde{F}^{n}_{j,k+\frac{1}{2}} + \tilde{G}^{n}_{j+\frac{1}{2},k+1} - \tilde{G}^{n}_{j+\frac{1}{2},k}] + \frac{\Delta t}{2}\hat{S}_{j+\frac{1}{2},k+\frac{1}{2}} \quad (3.11)$$

(first step)

$$W^{n+1}_{j,k} = W^{n}_{j,k} + \lambda[\tilde{F}^{n+\frac{1}{2}}_{j+\frac{1}{2},k} - \tilde{F}^{n+\frac{1}{2}}_{j-\frac{1}{2},k} + \tilde{G}^{n+\frac{1}{2}}_{j,k+\frac{1}{2}} - \tilde{G}^{n+\frac{1}{2}}_{j,k-\frac{1}{2}}] + \Delta t\, \tilde{S}^{n+\frac{1}{2}}_{j,k} \quad \text{(second step)} \quad (3.12)$$

where

$$\hat{S}_{j+\frac{1}{2},k+\frac{1}{2}} = \frac{1}{4}[S^{n}_{j+1,k+1} + S^{n}_{j+1,k} + S^{n}_{j,k+1} + S^{n}_{j,k}] \quad (3.13)$$

$$\tilde{S}^{n+\frac{1}{2}}_{j,k} = \frac{1}{4}[S^{n+\frac{1}{2}}_{j+\frac{1}{2},k+\frac{1}{2}} + S^{n+\frac{1}{2}}_{j+\frac{1}{2},k-\frac{1}{2}} + S^{n+\frac{1}{2}}_{j-\frac{1}{2},k+\frac{1}{2}} + S^{n+\frac{1}{2}}_{j-\frac{1}{2},k-\frac{1}{2}}] \quad (3.14)$$

$$S^{n+\frac{1}{2}}_{j+\frac{1}{2},k+\frac{1}{2}} = S(W^{n+\frac{1}{2}}_{j+\frac{1}{2},k+\frac{1}{2}}) \quad . \quad (3.15)$$

The expressions for $\tilde{F}^{n}_{j+1,k+\frac{1}{2}}$, $\tilde{F}^{n+\frac{1}{2}}_{j+\frac{1}{2},k}$, $\tilde{G}^{n}_{j+\frac{1}{2},k+1}$, $\tilde{G}^{n+\frac{1}{2}}_{j,k+\frac{1}{2}}$ etc. are the same as in the cartesian case, Eqs. (3.5)-(3.8). The inhomogeneous vector S does not effect the (linear) numerical stability and the stability condition remains as in Eq. (3.10).

(iii) The Three Dimensional Case

The various difference expressions for this case are obvious extensions of the two-dimensional ones. The basic finite difference scheme approximating the system (2.9) is given by:

$$W^{n+}_{j+\frac{1}{2},k+\frac{1}{2},\ell+\frac{1}{2}} = \hat{W}^{n}_{j+\frac{1}{2},k+\frac{1}{2},\ell+\frac{1}{2}} + \frac{\lambda}{2}\left[\tilde{F}^{n}_{j+1,k+\frac{1}{2},\ell+\frac{1}{2}} - \tilde{F}^{n}_{j,k+\frac{1}{2},\ell+\frac{1}{2}} + \tilde{G}^{n}_{j+\frac{1}{2},k+1,\ell+\frac{1}{2}} - \tilde{G}^{n}_{j+\frac{1}{2},k,\ell+\frac{1}{2}} + \tilde{H}^{n}_{j+\frac{1}{2},k+\frac{1}{2},\ell+1} - \tilde{H}^{n}_{j+\frac{1}{2},k+\frac{1}{2},\ell}\right] \quad \text{(first step)} \tag{3.16}$$

$$W^{n+1}_{j,k,\ell} = W^{n}_{j,k,\ell} + \lambda\left[\tilde{F}^{n+\frac{1}{2}}_{j+\frac{1}{2},k,\ell} - \tilde{F}^{n+\frac{1}{2}}_{j-\frac{1}{2},k,\ell} + \tilde{G}^{n+\frac{1}{2}}_{j,k+\frac{1}{2},\ell} - \tilde{G}^{n+\frac{1}{2}}_{j,k-\frac{1}{2},\ell} + \tilde{H}^{n+\frac{1}{2}}_{j,k,\ell+\frac{1}{2}} - \tilde{H}^{n+\frac{1}{2}}_{j,k,\ell-\frac{1}{2}}\right] \quad \text{(second step)} \tag{3.17}$$

where $$\lambda = \Delta t/\Delta x = \Delta t/\Delta y = \Delta t/\Delta z \tag{3.18}$$

$$\hat{W}^{n}_{j+\frac{1}{2},k+\frac{1}{2},\ell+\frac{1}{2}} = \frac{1}{8}\left[W_{j+1,k+1,\ell} + W_{j+1,k,\ell} + W_{j,k+1,\ell} + W_{j,k,\ell} + W_{j+1,k+1,\ell+1} + W_{j+1,k,\ell+1} + W_{j,k+1,\ell+1} + W_{j,k,\ell+1}\right] \tag{3.19}$$

$$\tilde{F}^{n}_{j+1,k+\frac{1}{2},\ell+\frac{1}{2}} = F\left(\frac{1}{4}\left(W^{n}_{j+1,k+1,\ell+1} + W^{n}_{j+1,k+1,\ell} + W^{n}_{j+1,k,\ell+1} + W^{n}_{j+1,k,\ell}\right)\right) \tag{3.20}$$

$$\tilde{F}^{n+\frac{1}{2}}_{j+\frac{1}{2},k,\ell} = F\left(\frac{1}{4}\left(W^{n+\frac{1}{2}}_{j+\frac{1}{2},k+\frac{1}{2},\ell+\frac{1}{2}} + W^{n+\frac{1}{2}}_{j+\frac{1}{2},k+\frac{1}{2},\ell-\frac{1}{2}} + W^{n+\frac{1}{2}}_{j+\frac{1}{2},k-\frac{1}{2},\ell+\frac{1}{2}} + W^{n+\frac{1}{2}}_{j+\frac{1}{2},k-\frac{1}{2},\ell-\frac{1}{2}}\right)\right) \tag{3.21}$$

$$\tilde{G}^{n}_{j+\frac{1}{2},k+1,\ell+\frac{1}{2}} = G\left(\frac{1}{4}\left(W^{n}_{j+1,k+1,\ell+1} + W^{n}_{j+1,k+1,\ell} + W^{n}_{j,k+1,\ell+1} + W^{n}_{j,k+1,\ell}\right)\right) \tag{3.22}$$

$$\tilde{G}^{n+\frac{1}{2}}_{j,k+\frac{1}{2},\ell} = G\left(\frac{1}{4}\left(W^{n+\frac{1}{2}}_{j+\frac{1}{2},k+\frac{1}{2},\ell+\frac{1}{2}} + W^{n+\frac{1}{2}}_{j+\frac{1}{2},k+\frac{1}{2},\ell-\frac{1}{2}} + W^{n+\frac{1}{2}}_{j-\frac{1}{2},k+\frac{1}{2},\ell+\frac{1}{2}} + W^{n+\frac{1}{2}}_{j-\frac{1}{2},k+\frac{1}{2},\ell-\frac{1}{2}}\right)\right) \tag{3.23}$$

$$\tilde{H}^{n}_{j+\frac{1}{2},k+\frac{1}{2},\ell+1} = H\left(\frac{1}{4}\left(W^{n}_{j+1,k+1,\ell+1} + W^{n}_{j+1,k,\ell+1} + W^{n}_{j,k+1,\ell+1} + W^{n}_{j,k,\ell+1}\right)\right) \tag{3.24}$$

$$\tilde{H}^{n+\frac{1}{2}}_{j,k,\ell+\frac{1}{2}} = H\left(\frac{1}{4}\left(W^{n+\frac{1}{2}}_{j+\frac{1}{2},k+\frac{1}{2},\ell+\frac{1}{2}} + W^{n+\frac{1}{2}}_{j+\frac{1}{2},k-\frac{1}{2},\ell+\frac{1}{2}} + W^{n+\frac{1}{2}}_{j-\frac{1}{2},k+\frac{1}{2},\ell+\frac{1}{2}} + W^{n+\frac{1}{2}}_{j-\frac{1}{2},k-\frac{1}{2},\ell+\frac{1}{2}}\right)\right), \tag{3.25}$$

with similar expressions for different subscripts. By anology to (3.10) the largest time step allowable under the (linear) stability criterion is

$$\Delta t_{n+1} = t_{n+1} - t_n \leq \frac{\Delta x}{\max\limits_{j,k,\ell}\left[c^{n}_{j,k,\ell} + \sqrt{(u^{n}_{j,k,\ell})^2 + (v^{n}_{j,k,\ell})^2 + (w^{n}_{j,k,\ell})^2}\right]} \tag{3.26}$$

(iv) The Treatment of Shock Waves by an Automatic Numerical "Switch"

In most of the flow field, the 2-D and 3-D algorithm - Eqs.(3.1)+(3.2) and (3.16)+(3.17) and the cylindrical symmetry algorithm - Eqs. (3.11)+(3.12) - give results which are linearly stable and which are of second order accuracy. In the vicinity of shock waves and stagnation points there exists (for different reasons) the danger of *non-linear* numerical instability. Harten and Zwas, [6], ameliorate this phenomenon by a modified application of the Shuman filter. Usually (see Vliegenthart [13]) the filtering is applied to the whole flow field and this reduces the accuracy of the algorithm to first order. If, however, the filtering is done only in the immediate vicinity of a shock wave, then the non-linear instability is usually prevented while the accuracy of the computation in the rest of the flow field remains of second order.

In the two-dimensional and the cylindrically symmetric cases one proceeds as follows:

$$W^{n+1}_{j,k} = L\,\bar{W}^{n}_{j,k} \tag{3.27}$$

$$\bar{\bar{W}}^{n+1}_{j,k} = W^{n+1}_{j,k} + \frac{1}{4}\left[\theta^{x}_{j+\frac{1}{2},k}\left(W^{n+1}_{j+1,k} - W^{n+1}_{j,k}\right) - \theta^{x}_{j-\frac{1}{2},k}\left(W^{n+1}_{j,k} - W^{n+1}_{j-1,k}\right)\right]$$

$$+ \frac{1}{4}\left[\theta^{y}_{j,k+\frac{1}{2}}\left(W^{n+1}_{j,k+1} - W^{n+1}_{j,k}\right) - \theta^{y}_{j,k-\frac{1}{2}}\left(W^{n+1}_{j,k} - W^{n+1}_{j,k-1}\right)\right]. \tag{3.28}$$

Where the operator L is the scheme (3.1)+(3.2), or in the cylindrical symmetry case, the scheme (3.11)+(3.12). The "switches" θ^{y}, θ^{x} are defined as follows:

$$\theta^{x}_{j+\frac{1}{2},k} = \chi\left[\frac{|\rho_{j+1,k} - \rho_{j,k}|}{\max_{j,k}|\rho_{j+1,k} - \rho_{j,k}|}\right]^{m}, \tag{3.29}$$

$$\theta^{y}_{j,k+\frac{1}{2}} = \chi\left[\frac{|\rho_{j,k+1} - \rho_{j,k}|}{\max_{j,k}|\rho_{j,k+1} - \rho_{j,k}|}\right]^{m}. \tag{3.30}$$

Near shock waves, or other regions of very strong gradients, the expressions in the square brackets in (3.29) and (3.30) are of order unity and then θ^x, $\theta^y \simeq \chi$ and the filtering defined by (3.28) becomes operative. Away from the shock-wave, the flow is smooth and $\theta^{x,y} \simeq 0[(\Delta x)^m]$. Thus, for $m \geq 1$, in the smooth regions $\bar{\bar{W}}^{n+1}_{j,k} = W^{n+1}_{j,k} + 0(\Delta x^2)$ at least; i.e. second order accuracy is preserved. In practice, one uses the scheme (3.27)+(3.28) with the θ^x's and θ^y's substituted from (3.29) and (3.30). Because of linear stability requirements we are constrained to use $0 < \chi \leq 1$.

In the three dimensional case Eq. (3.28) takes the form

$$\begin{aligned}\bar{\bar{W}}^{n+1}_{j,k,\ell} = W^{n+1}_{j,k,\ell} &+ \frac{1}{4}[\theta^{x}_{j+\frac{1}{2},k,\ell}(W^{n+1}_{j+1,k,\ell} - W^{n+1}_{j,k,\ell}) - \theta^{x}_{j-\frac{1}{2},k,\ell}(W^{n+1}_{j,k,\ell} - W^{n+1}_{j-1,k,\ell})] \\ &+ \frac{1}{4}[\theta^{y}_{j,k+\frac{1}{2},\ell}(W^{n+1}_{j,k+1,\ell} - W^{n+1}_{j,k,\ell}) - \theta^{y}_{j,k-\frac{1}{2},\ell}(W^{n+1}_{j,k,\ell} - W^{n+1}_{j,k-1,\ell})] \\ &+ \frac{1}{4}[\theta^{z}_{j,k,\ell+\frac{1}{2}}(W^{n+1}_{j,k,\ell+1} - W^{n+1}_{j,k,\ell}) - \theta^{z}_{j,k,\ell-\frac{1}{2}}(W^{n+1}_{j,k,\ell} - W^{n+1}_{j,k,\ell-1})]\end{aligned} \tag{3.28a}$$

where $\theta^{x}_{j+\frac{1}{2},k,\ell}$ and $\theta^{y}_{j,k+\frac{1}{2},\ell}$ are defined respectively according to (3.29) and (3.30) suitably modified, and

$$\theta^{z}_{j,k,\ell+\frac{1}{2}} = \chi \left[\frac{|\rho_{j,k,\ell+1} - \rho_{j,k,\ell}|}{\max_{j,k,\ell} |\rho_{j,k,\ell+1} - \rho_{j,k,\ell}|} \right]^{m} . \tag{3.31}$$

Also, linear stability analysis [6], shows that in contradistinction to the two dimensional and cylindrical symmetric cases, in the three dimensional case the filtering coefficient χ has a more restricted range. Specifically, in the 3-D case we are constrained to use $0 < \chi \leq 2/3$.

4. TREATMENT OF BOUNDARY AND INITIAL CONDITIONS

(i) Boundaries That Are Not on The Body

The computation is usually done over a rectangular grid of $J \times K$ net points, where J is the number of grid points in the x-direction and K is the number in the y or r direction. We choose K in such a way that the bow shock wave will not cross the upper boundary, $k = K$ (the lower boundary, $k = 1$, is usually taken along the axis of symmetry) but the right hand boundary, $j = J$. (See sketch.)

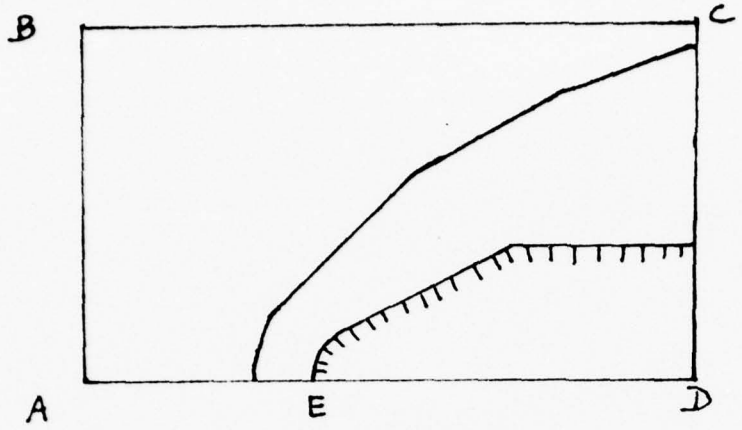

Along BC the boundary conditions are found by extrapolation along 45° lines except that very near to B (2 points along BC) where the extrapolation is in a direction perpendicular to BC. Along CF we use the same strategy except that very near F the extrapolation is in a direction parallel to the body surface. Along AE the boundary conditions are determined by the symmetry of the flow (zero angle of attack).

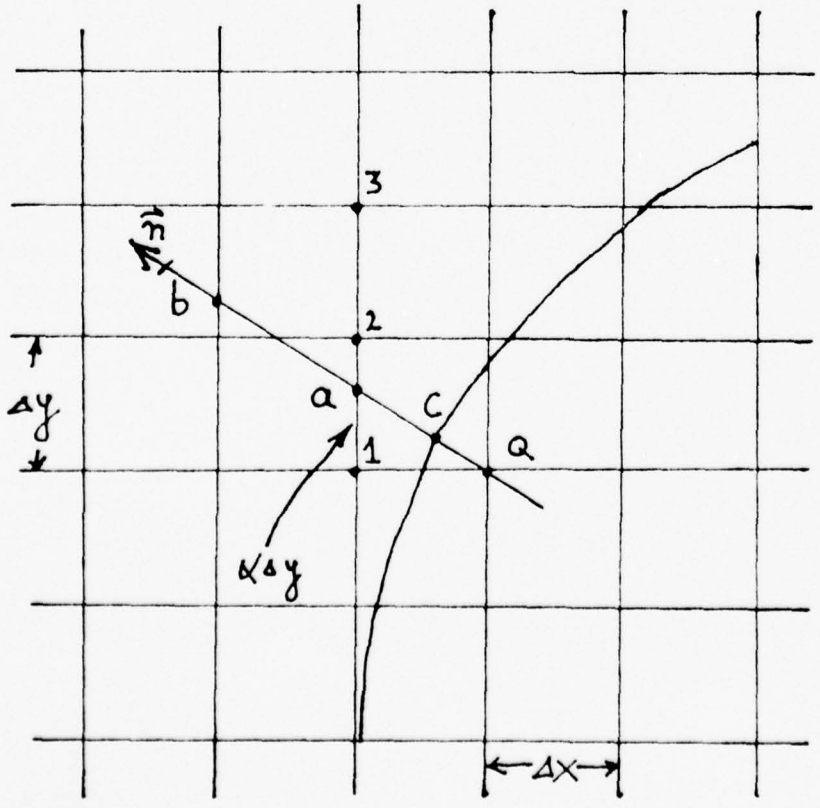

If the flow is not symmetric about the x-axis (angle of attack is not zero) then for the lower boundary we use not AE but a line B'C' which we treat in the same manner as BC. On the boundary AB we set fixed the ambient free stream conditions of the steady state flow which we are trying to model.

(ii) Boundary Conditions on the Surface of a Two-Dimensional Body

One way of dealing with boundary conditions on a body of arbitrary shape is to transform the computational grid in such a fashion that the body surface then coincides with one of the new coordinates. The difficulty with this is that the finite difference algorithm becomes more complex and has to be changed to fit each new problem. We chose, on the other hand, to stay with the convenience of a rectangular mesh. Of course, we then face the problem that the body surface does not, in general, pass through grid points. (See sketch on previous page.)

We need to know the components of W at the point "Q" (inside the body) at time t_n in order to be able to compute, for example, W at point "2" (outside the body) at time $t_{n+1} = t_n + \Delta t_n$. The points "a" and "b" were chosen in such a way that the line Qab is normal to the body at the point of intersection, "c". For the purpose of the discussion in this section only, let f be any component of W or of the related vector (ρ, u, v, E). When f stands for either the density, energy or the velocity in the direction of the tangent to the body at "c" we find its value at Q by using a "parabolic reflection". Namely, we pass a parabola through the points a, b and Q so that the derivative in the direction of the normal Qab is zero at the point "c". This is done by setting

$$f_Q = \frac{f_b - f_a}{\ell_b^2 - \ell_a^2} (\ell_Q^2 - \ell_a^2) + f_a \ , \tag{4.1}$$

where ℓ_a, ℓ_b and ℓ_Q are the distances of the points "a", "b" and "Q" from the point "c". The values of f_a and f_b are found from parabolic interpolation among the grid points nearest to them. Thus

$$f_a = \frac{1}{2}(\alpha-1)(\alpha-2)f_1 - \alpha(\alpha-2)f_2 + \frac{\alpha(\alpha-1)}{2} f_3 \ , \tag{4.2}$$

where $\alpha\Delta y$ is the distance of point "a" from point "1", etc. When f stands for the velocity in the direction normal to the body, it must vanish at point "c". We satisfy this condition through a parabolic extrapolation that yields for f_Q the value

$$f_Q = \ell_Q [(\frac{f_a}{\ell_a} - \frac{f_b}{\ell_b}) \frac{\ell_Q - \ell_a}{\ell_a - \ell_b} + \frac{f_a}{\ell_a}] \ . \tag{4.3}$$

(iii) Boundary Conditions on the Surface of a Body of Revolution

The philosophy of the treatment is the same as in Section 4- (ii) except that where the radius of curvature of the body is finite we use instead of parabolic reflection and extrapolation linear ones. This helps with the stability and leaves the overall accuracy unchanged. Thus we replace (4.1)+(4.2) by (4.4)+(4.2):

$$f_Q = f_a + \frac{\ell_Q - \ell_a}{\ell_b - \ell_a} (f_b - f_a) \ , \tag{4.4}$$

while (4.3) is replaced by

$$f_Q = - \left[f_a + \frac{\ell_Q - \ell_a}{\ell_b - \ell_a} (f_b - f_a) \right] \quad . \tag{4.5}$$

Note that even though the finite difference system is solved for $W' = rW$, the conditions (4.4) and (4.5) are applied to the physical qualities $W = W'/r$.

Near the axis of symmetry, $r = 0$, we have the problem of $W' = 0$ there. To compute W on the axis we use the known values at $r = \Delta r$ $r = 2\Delta r$ and $r = -\Delta r$ and interpolate. Finally, note that also on boundaries away from the body surface, such as BC for example, all extrapolations are done on W and not on W'.

(iv) Initial Conditions

At $t = 0$ the whole flow field is assigned the free stream conditions. We chose to nondimensionalize in such a way that both the free stream pressure and density take on the value of 1. Thus the free stream sound speed becomes $c_\infty = \sqrt{\gamma}$.

When we did parametric runs the conditions at $t = 0$ were set to the converged solution of a similar run thus saving computation time.

5. NUMERICAL RESULTS

The numerical results were obtained for several problems.

(i) Steady, two dimensional, supersonic flow past a circularly blunted wedge with a semi-apex angle of 13°, at zero angle of attack.

(ii) Steady, cylindrically symmetric, supersonic flow past a spherically blunted cone with a semi-apex solid angle of 13°, at zero angle of attack.

In both of the above groupings the computations were carried out for free stream Mach number range of $2 \leq M_\infty \leq 4$ with jumps of $\Delta M_\infty = 0.5$ from one run to another. The graphs show the distribution along the body of the ratio of surface pressure to the stagnation point pressure and the distribution of the surface local Mach number.

The Mach number distribution over the wedge is shown in Figs. 2 - 6. The pressure distribution over the wedge is shown in Figs. 7 - 11. The pressure distribution over the cone is shown in Figs. 12 - 16. The Mach number distribution over the cone is shown in Figs. 17 - 21. At the top of Figs. 2, 7, 12 and 17, each at $M_\infty = 2$, is shown the body shape over which the calculation was done.

The surface pressure over the body was computed in two ways: directly from the finite difference scheme and also by assuming that the body represents a stream tube over which there is isentropic flow and hence the pressure over it is related directly to the (local) surface Mach

number. In Fig. 12, for example, we show the pressure as computed by both approaches. The dashed-line curve gives the pressure ratio as obtained directly from the finite difference equation and the undashed curve corresponds to the "isentropic" calculation. It is seen that the results are nearly identical except near the front of the cone where the calculations are affected by the small r value. Because of the agreement between the two methods, we show on most graphs only pressure distribution curve.

All the two dimensional calculations were done on a grid of 52x55 (J = 52, K = 55). Running time, when the initial conditions correspond everywhere to the free stream value is about 25 minutes (there are some variations depending on Mach number, wedge angle, etc.). But if, for example, for the $M_\infty = 2.5$ run we use as initial conditions the numerical solution from the $M_\infty = 2.0$ run, then the running time decrease to about 10 minutes. We thus found that the *average* running time per case, for computing the cases $M_\infty = 2, 2.5, 3, 3.5, 4$ is about 12 minutes.

For the flow around the blunted cone we used a net of 65x64 grid points and the computation time was roughly the same as in the cartesian case.

In order to compare our algorithm with other numerical techniques we made use of the results obtained from semi-empirical computer programs based on Russian data for a blunt cone with 10° semi-apex angle at $M_\infty = 3$. This information is contained in a 1966 AVCO Report

no. SR 10-TR-66-47 written by R.H. Kohrs. We ran calculations for the same configuration. The comparison is shown in Fig. 22. It is seen that the agreement is very good.

(iii) In Fig. 23 we show the results for our blunted wedge but at an angle of attack of 5°. The distributions are shown for both the upper and lower surfaces.

In all of the above runs we used a linear Shuman filter, i.e. we took $m = 1$ in equations 3.18 and 3.19. The dissipation coefficient χ was taken to be 1/2 in the two dimensional calculations. In the axisymmetric case the value of χ was varied to get best results for the stagnation density and was found to be $.9 \leq \chi < 1.0$.

(iv) Finally, we tested our 3-D package by applying it to the problem of the supersonic flow past a body composed of a hemisphere followed by a circular cylinder, at a zero angle of attack.

This allowed us to check how the results obtained, using a 3-D algorithm compare with those given by a (two-dimensional) axisymmetric scheme. The computational net was 42x40x40. Thus we had 67,200 mesh points as compared to the 4,225 points of the 65x65 "2-D" mesh. In addition, in each mesh point in the 3-D case we have to store a 5-vector $(\rho, \rho u, \rho v, \rho w, E)$ as compared to the 4-vector $(\rho, \rho u, \rho v, E)$ in the axisymmetric case. Thus the storage requirements in the 3-D case exceed by a factor of 20 (twenty) those of the 2-D case. Since this requirement exceeds the core-memory capacity, we used discs for the

mass-storage. Here we utilized the hyperbolic nature of the p.d.e. system: as each field point was computed, its "cube (3x3x3) of influence" was moved by one mesh point freeing core-memory storage for data to be transfered from the disc. The data transfer can be done while the arithmetic unit carries out the computation. In this manner the effect of the slow rate of transfer is mitigated. In fact, a typical run took 12 times longer than the corresponding 2-D calculation (all with the above given mesh sizes). The "improved" efficiency (12 vs. 20) is due to the coarser mesh (1/40 vs. 1/65). The pressure distribution thus obtained agrees well with the axisymmetric results. Typically, while the stagnation pressure was under-predicted by about 3% in the axisymmetric calculation, it was over-predicted by about 4% in the 3-D runs. The drag coefficient

$$C_D = \frac{D}{\frac{1}{2}\rho_\infty U_\infty^2 \pi R^2} = \frac{2}{\gamma M_\infty^2} \left(\frac{p_{stg}}{p_\infty}\right) \iint \left(\frac{p}{p_{stg}}\right) \frac{dA}{\pi R^2}$$

was calculated in both cases. Typical values, at $M_\infty = 3$, are

$$C_D = 0.98 \qquad \text{(axisymmetric)}$$

$$C_D = 1.04 \qquad \text{(3-D)} \quad .$$

We conclude therefore, that our 3-D algorithm is apparently reliable and we now plan to apply it to truly three dimensional flow, i.e. in the case of non-zero angle of attack.

ACKNOWLEDGEMENT: Many thanks are due to Ms. Dora Raber who carried out the scientific programming.

REFERENCES

[1]a) Dorodnitsyn, A.A. "On a Method of Numerical Solution of Some Nonlinear Problems of Aerodynamics" Proc. 9th International Congress on Applied Mechanics, Brussels, vol.1 (1957), p. 485.

b) Belotserkovskii, O.M.
Dokl. Akad. Nank SSSR, 113 (1957), pp. 509-512.

[2] Garabedian, P.R.
J. Math. Phys., 36 (1957), pp. 192-205.

[3] Lax, P.D. and Wendroff, B.
Comm. Pure Appl. Math., 17 (1964), pp. 381-392.

[4] Richtmyer, R.D. and Morton, K.W. "Finite Difference Methods for Initial Value Problems" Interscience Publications, (1967).

[5] Zwas, G.
Numer. Math., 20 (1973), pp. 350-355.

[6] Harten, A. and Zwas, G.
J. Eng. Math., 6 (1972), pp. 207-216.

[7] Abarbanel, S. and Gottlieb, D.
Math. Comp., 27 (1973), pp. 505-523.

[8] Goldberg, M. and Abarbanel, S.
Math. Comp., 28 (1974), pp. 413-447.

[9] Abarbanel, S. Gottlieb, D. and Turkel, E.
SIAM J. Appl. Math., 29 (1975), pp. 329-351.

[10] Turkel, E. Abarbanel, S. and Gottlieb, D.
J. Comp. Phys., 21 (1976), pp. 85-113.

[11] Burstein, S.Z. "High Order Accurate Difference Methods in Hydrodynamics" Nonlinear PDE, ed. F.Ames, Academic Press, N.Y. (1967), pp. 279-290.

[12] Burstein, S.Z. and Mirin, A.A.
J. Comp. Phys., 5 (1970), pp. 547-557.

[13] Vliengenthart, A.C.
J. Eng. Math., 4 (1970), pp. 341-348.

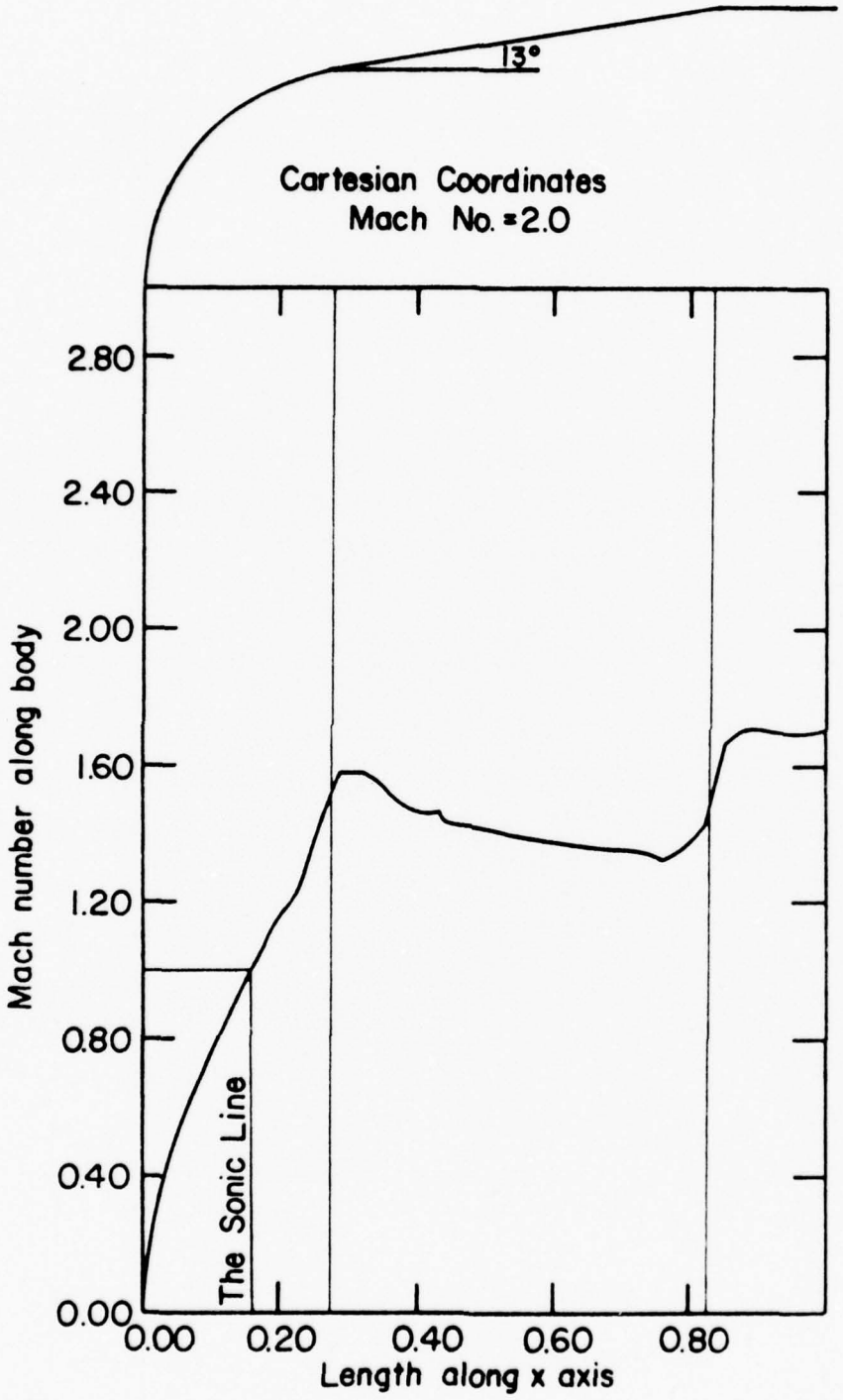
13°
Cartesian Coordinates
Mach No. = 2.0
2.80
2.40
2.00
1.60
1.20
0.80
0.40
0.00
Mach number along body
The Sonic Line
0.00
0.20
0.40
0.60
0.80
Length along x axis

Fig. 2

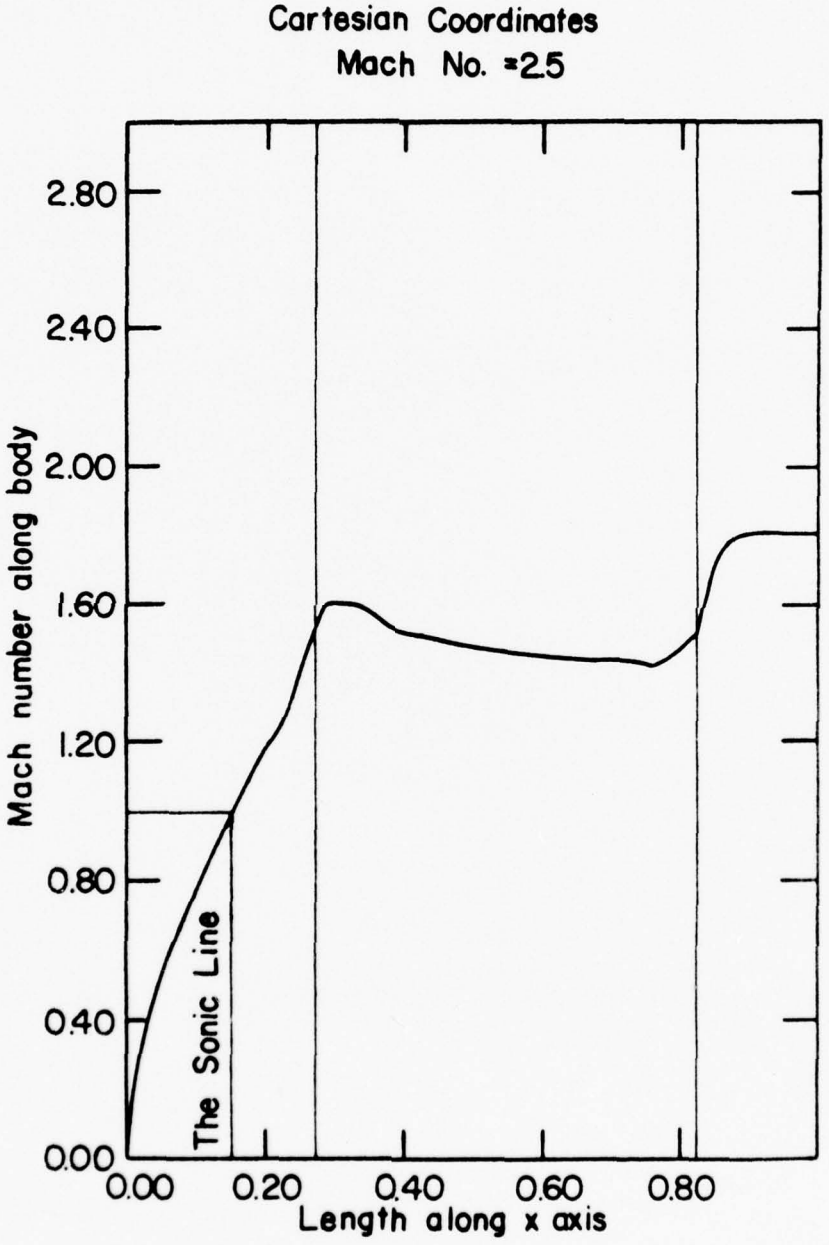
Cartesian Coordinates
Mach No. =2.5
Mach number along body
2.80
2.40
2.00
1.60
1.20
0.80
0.40
0.00
The Sonic Line
0.00
0.20
0.40
0.60
0.80
Length along x axis

Fig. 3

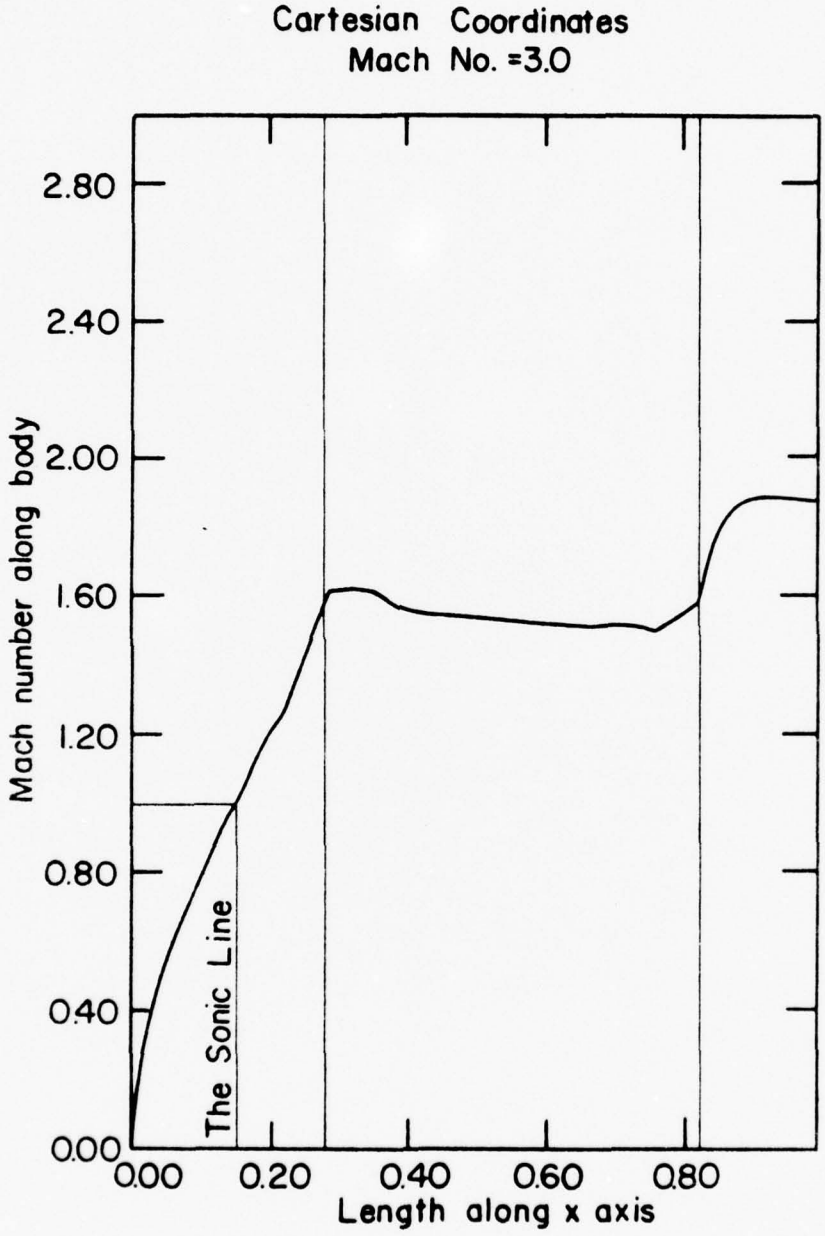
Cartesian Coordinates
Mach No. =3.0
Mach number along body
2.80
2.40
2.00
1.60
1.20
0.80
0.40
0.00
The Sonic Line
0.00
0.20
0.40
0.60
0.80
Length along x axis

Fig. 4

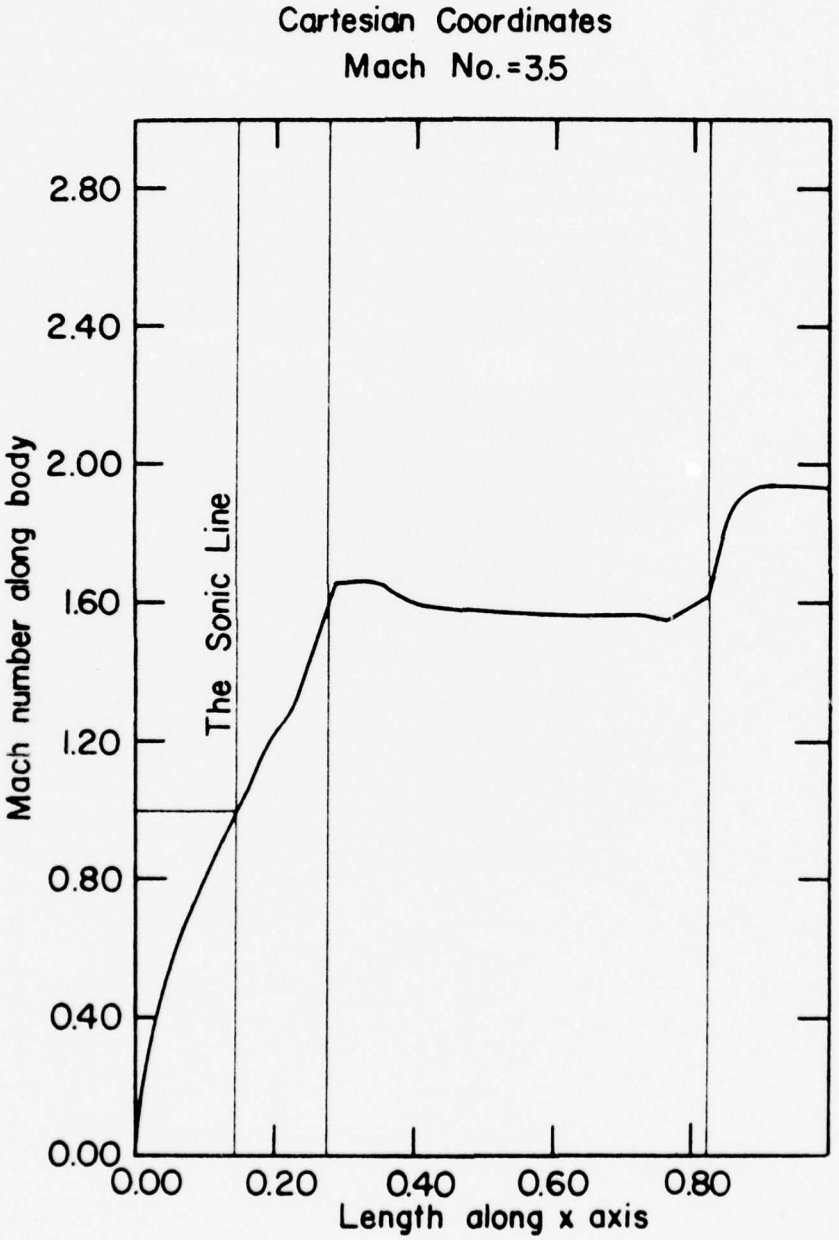
Cartesian Coordinates
Mach No.=3.5
Mach number along body
2.80
2.40
2.00
1.60
1.20
0.80
0.40
0.00
The Sonic Line
0.00
0.20
0.40
0.60
0.80
Length along x axis

Fig. 5

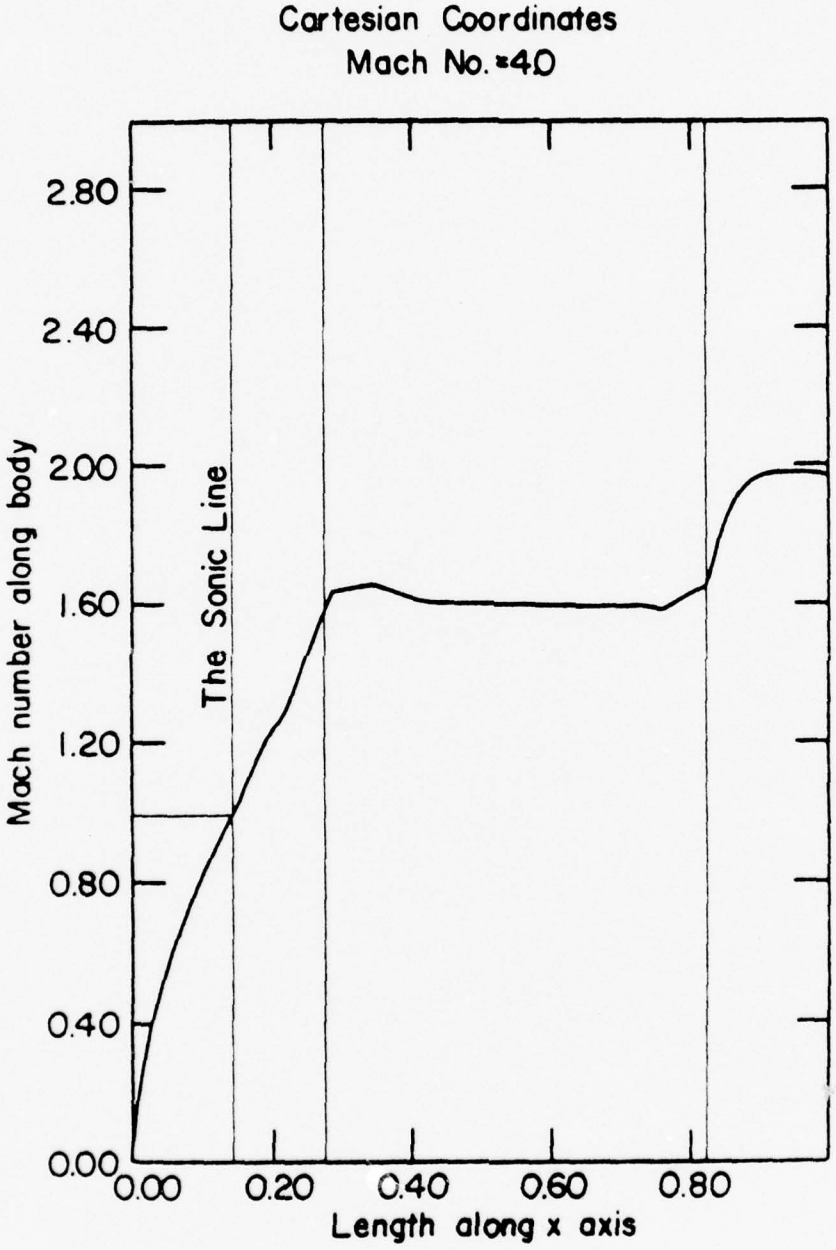
Cartesian Coordinates
Mach No. =4.0
Mach number along body
2.80
2.40
2.00
1.60
1.20
0.80
0.40
0.00
The Sonic Line
0.00
0.20
0.40
0.60
0.80
Length along x axis

Fig. 6

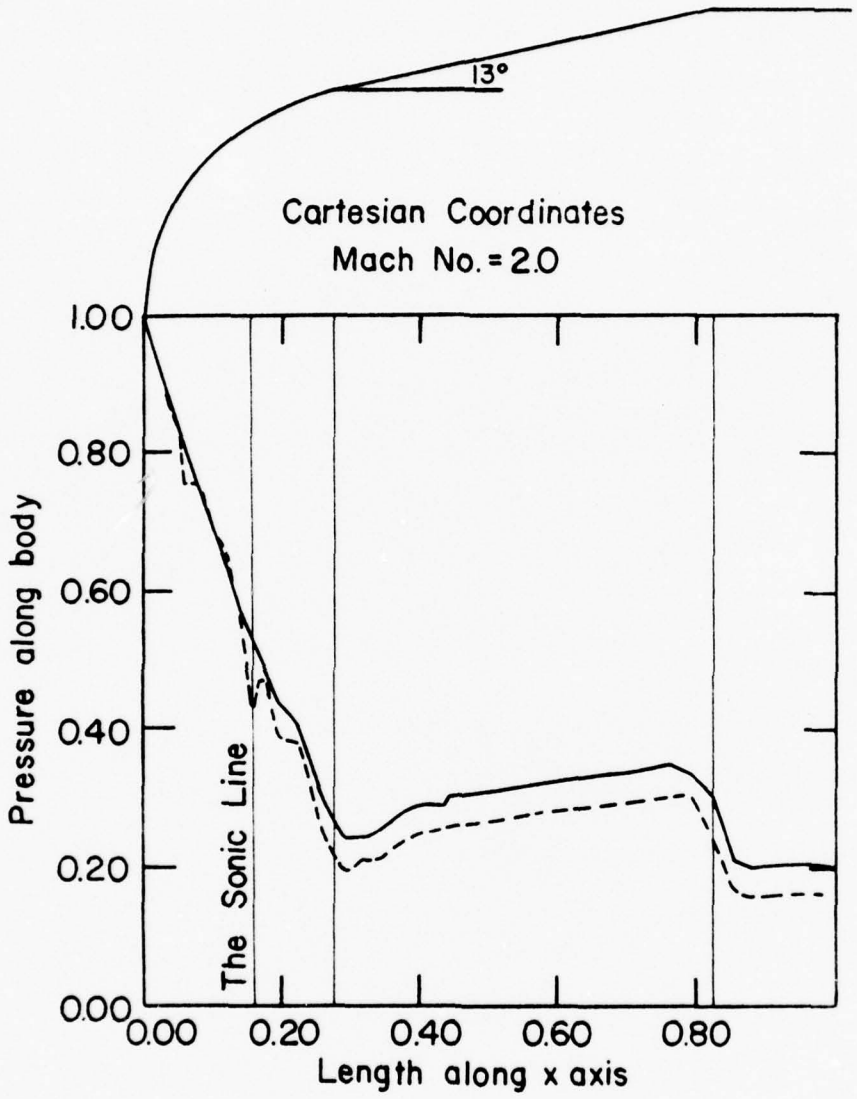
13°
Cartesian Coordinates
Mach No. = 2.0
1.00
0.80
0.60
0.40
0.20
0.00
Pressure along body
The Sonic Line
0.00
0.20
0.40
0.60
0.80
Length along x axis

Fig. 7

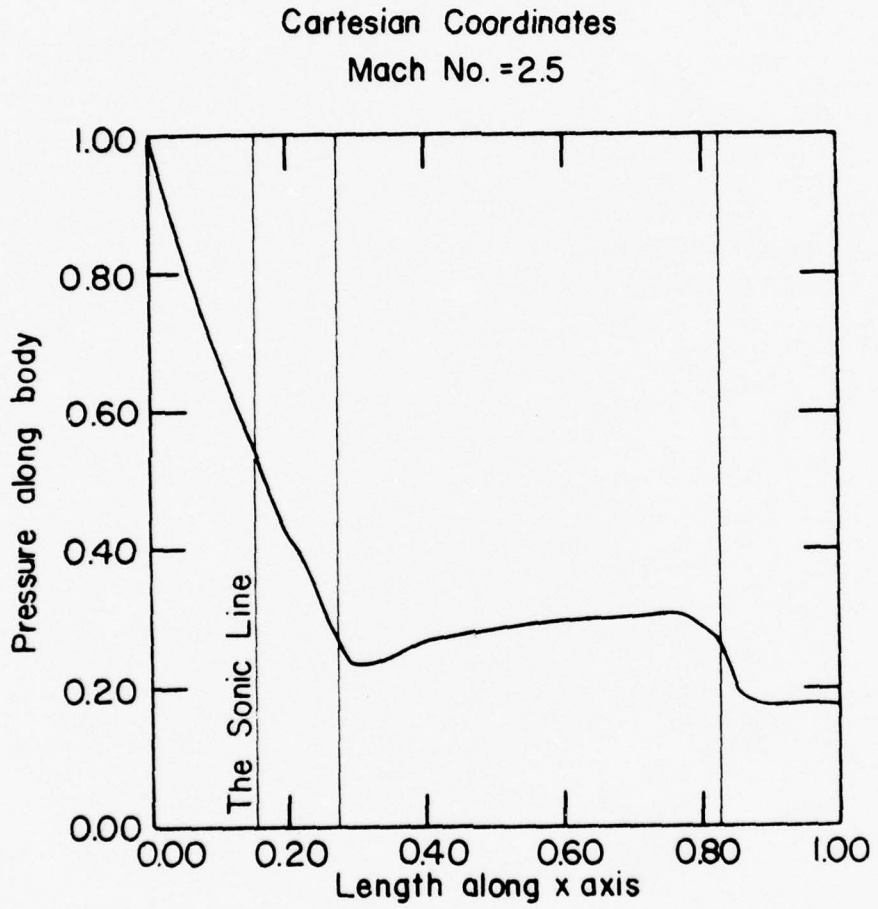
Cartesian Coordinates
Mach No. =2.5
Pressure along body
1.00
0.80
0.60
0.40
0.20
0.00
The Sonic Line
0.00
0.20
0.40
0.60
0.80
1.00
Length along x axis

Fig. 8

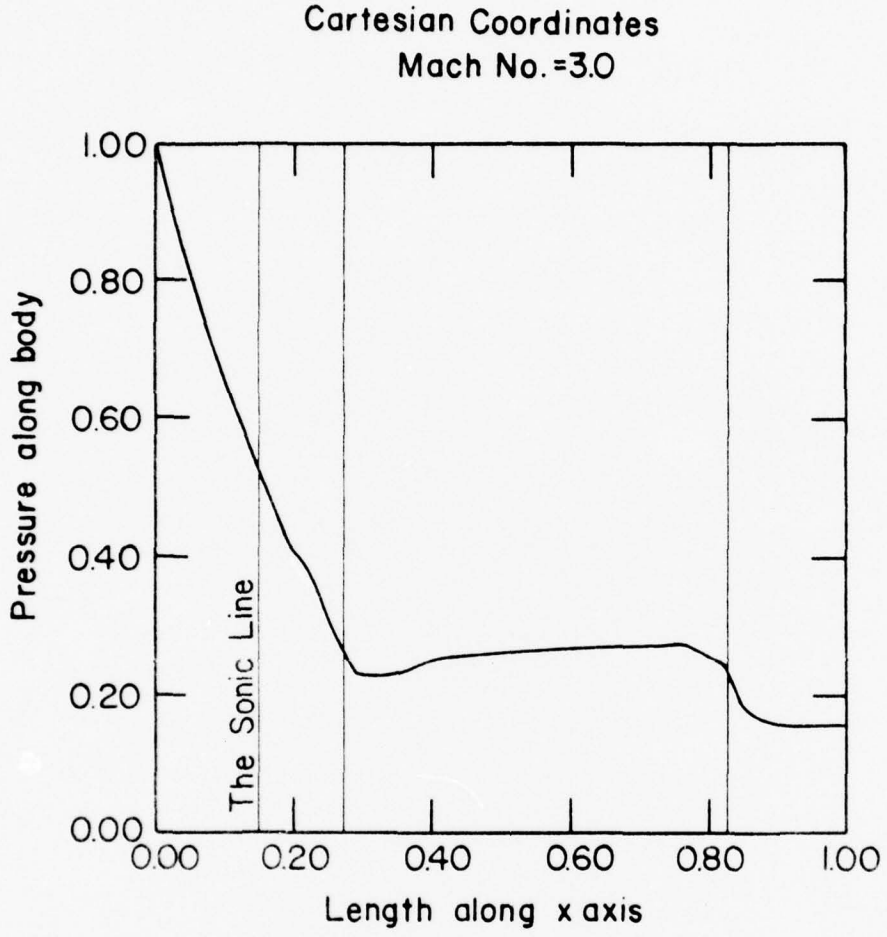
Cartesian Coordinates
Mach No. =3.0
Pressure along body
1.00
0.80
0.60
0.40
0.20
0.00
The Sonic Line
0.00
0.20
0.40
0.60
0.80
1.00
Length along x axis

Fig. 9

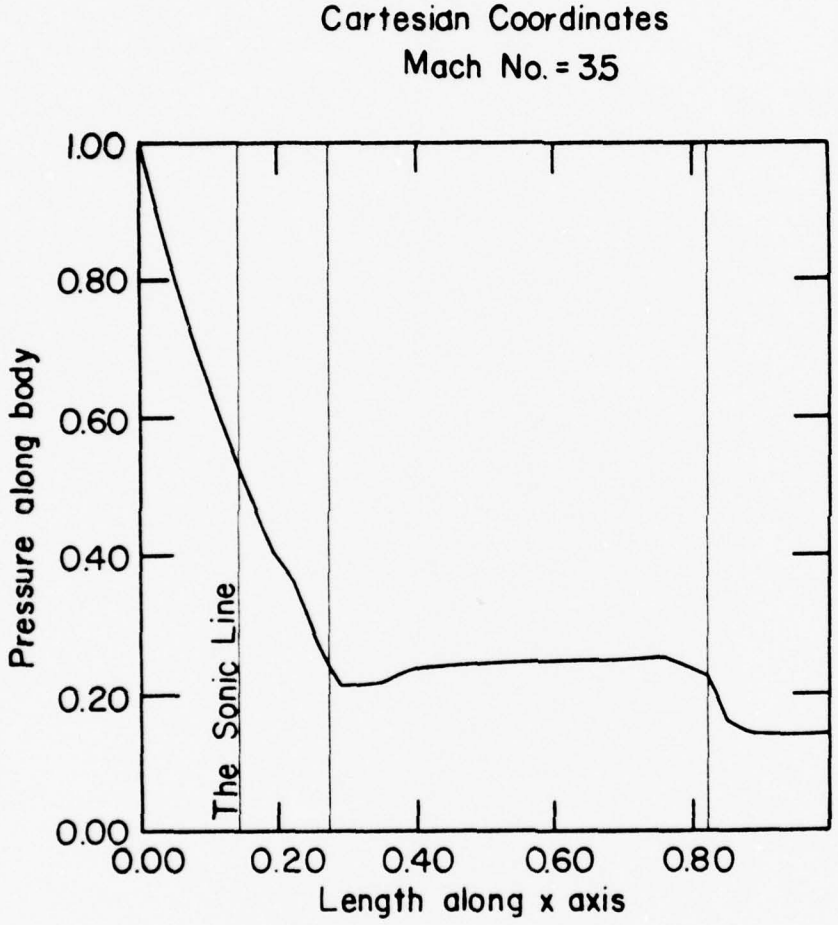
Cartesian Coordinates
Mach No. = 3.5
Pressure along body
1.00
0.80
0.60
0.40
0.20
0.00
The Sonic Line
0.00
0.20
0.40
0.60
0.80
Length along x axis

Fig. 10

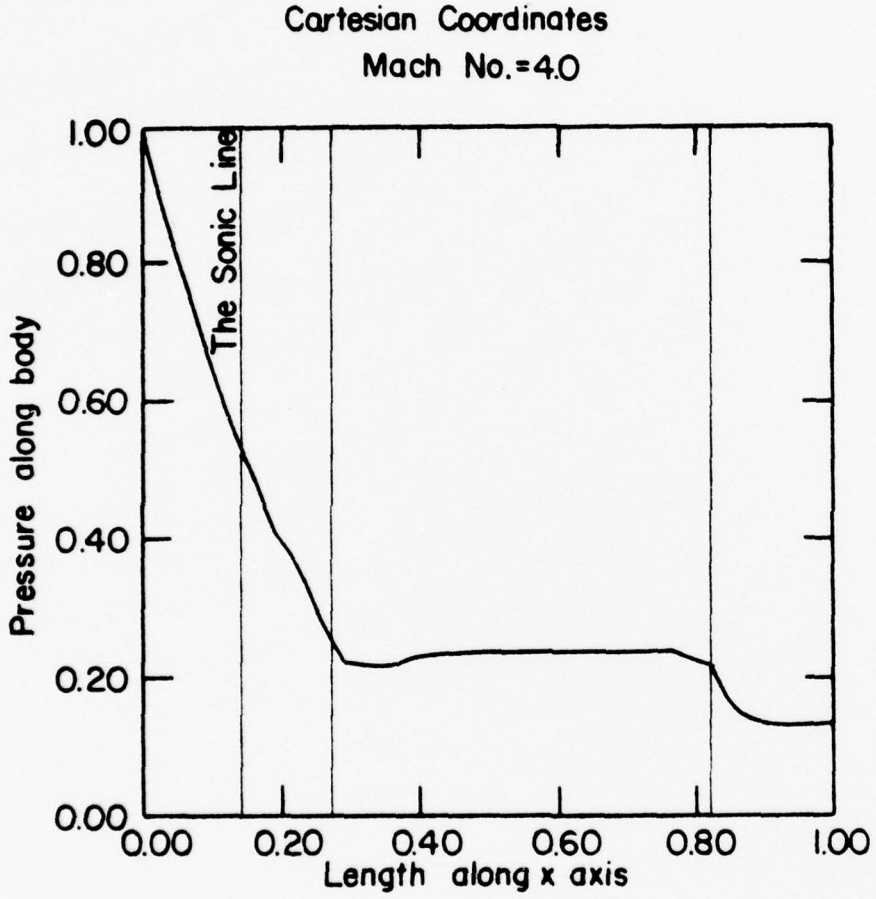
Cartesian Coordinates
Mach No.=4.0
The Sonic Line
Pressure along body
1.00
0.80
0.60
0.40
0.20
0.00
0.00
0.20
0.40
0.60
0.80
1.00
Length along x axis

Fig. 11

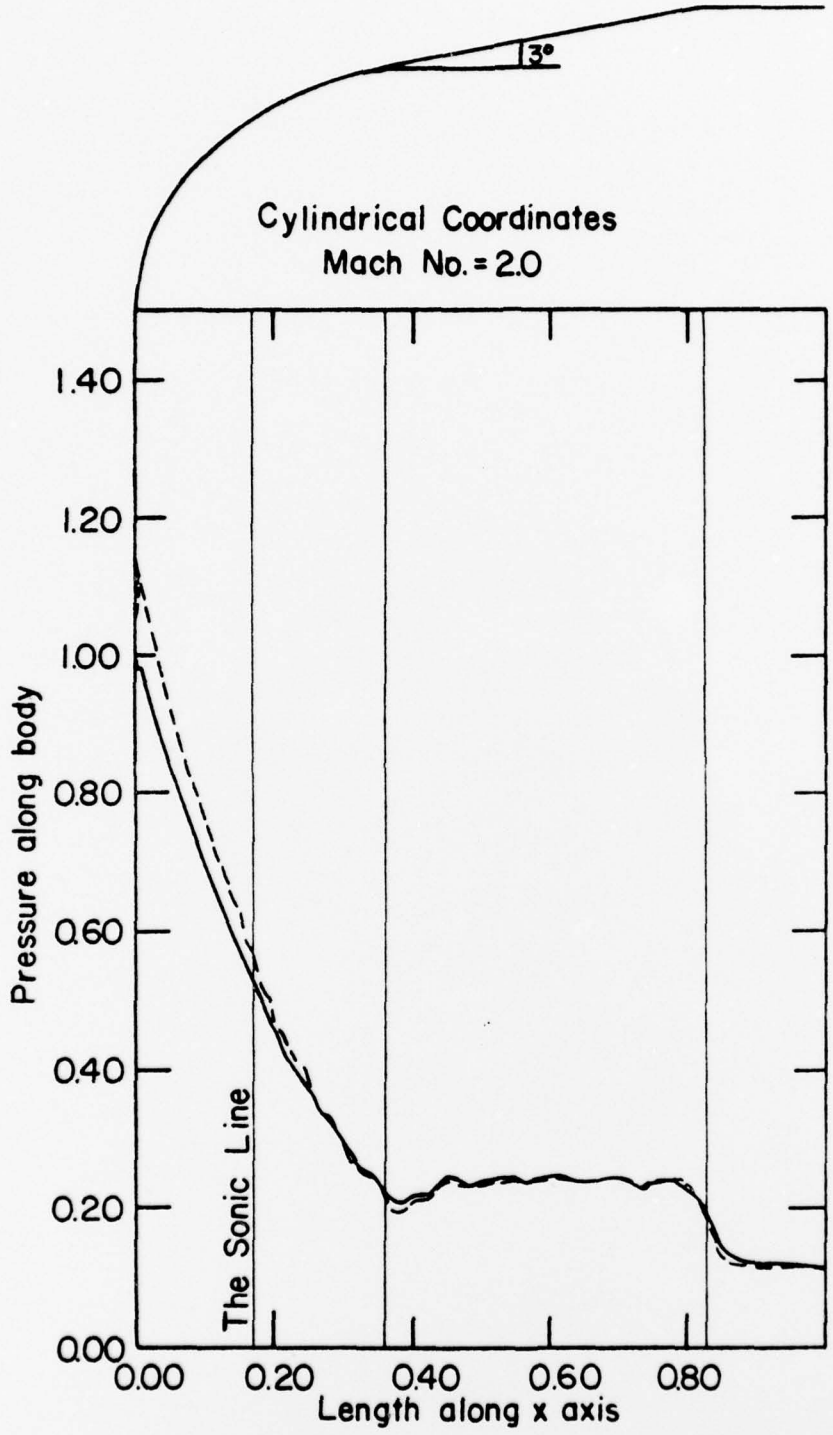
3°
Cylindrical Coordinates
Mach No. = 2.0
1.40
1.20
1.00
0.80
0.60
0.40
0.20
0.00
Pressure along body
The Sonic Line
0.00
0.20
0.40
0.60
0.80
Length along x axis

Fig. 12

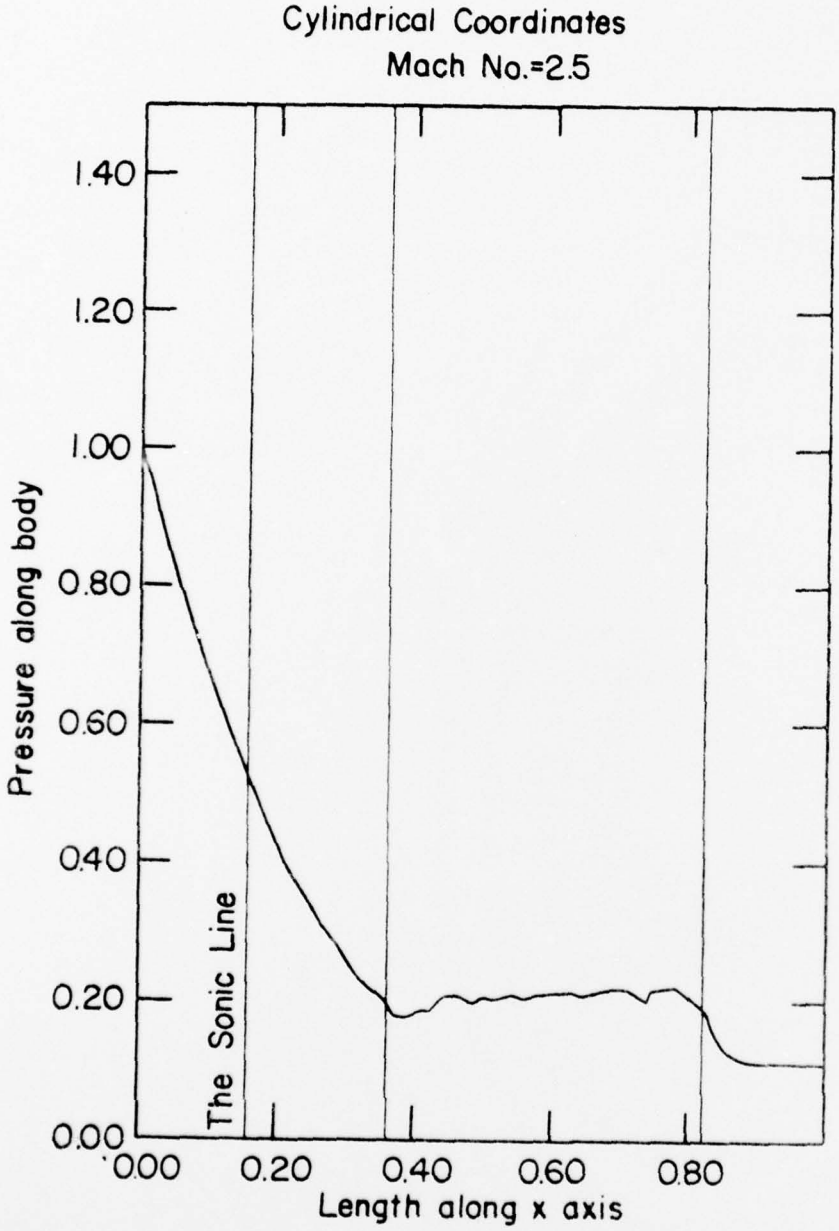
Cylindrical Coordinates
Mach No.=2.5
Pressure along body
1.40
1.20
1.00
0.80
0.60
0.40
0.20
0.00
The Sonic Line
0.00
0.20
0.40
0.60
0.80
Length along x axis

Fig. 13

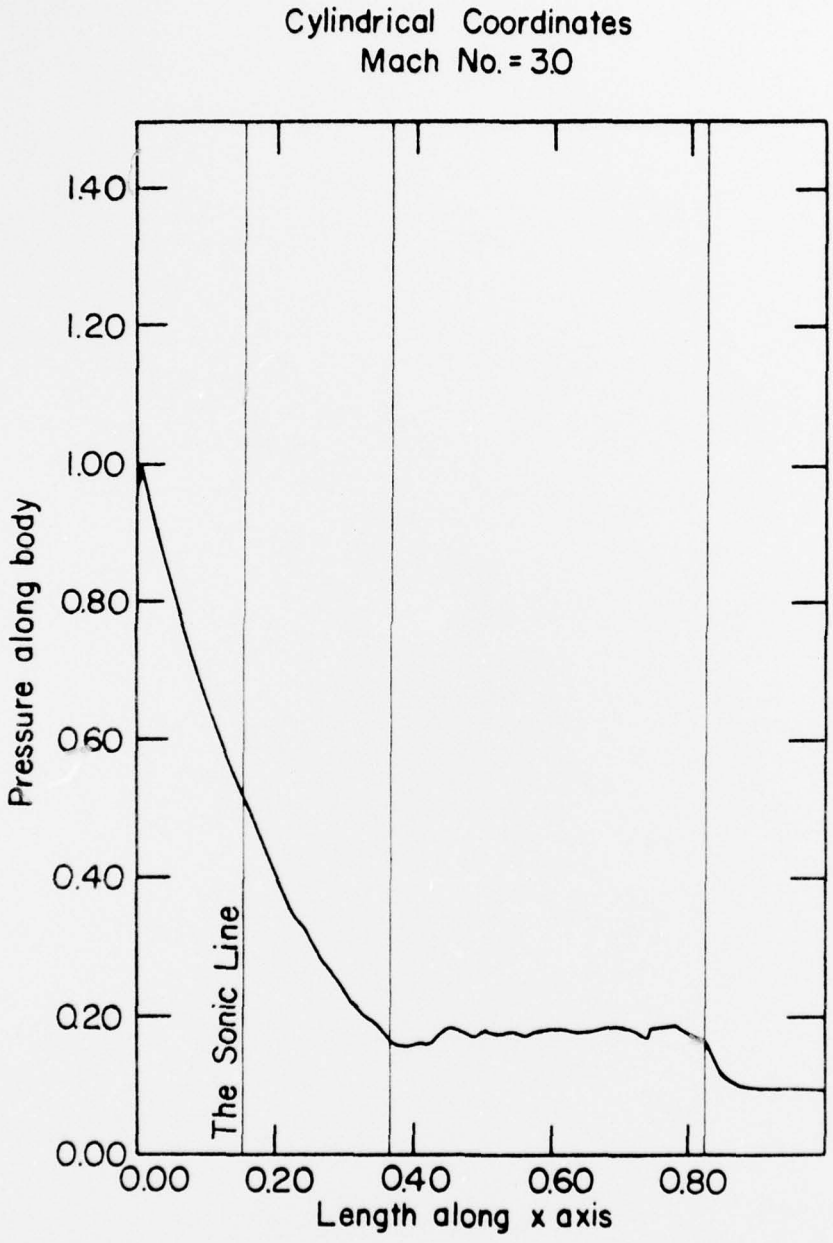
Cylindrical Coordinates
Mach No. = 3.0
Pressure along body
1.40
1.20
1.00
0.80
0.60
0.40
0.20
0.00
The Sonic Line
0.00
0.20
0.40
0.60
0.80
Length along x axis

Fig. 14

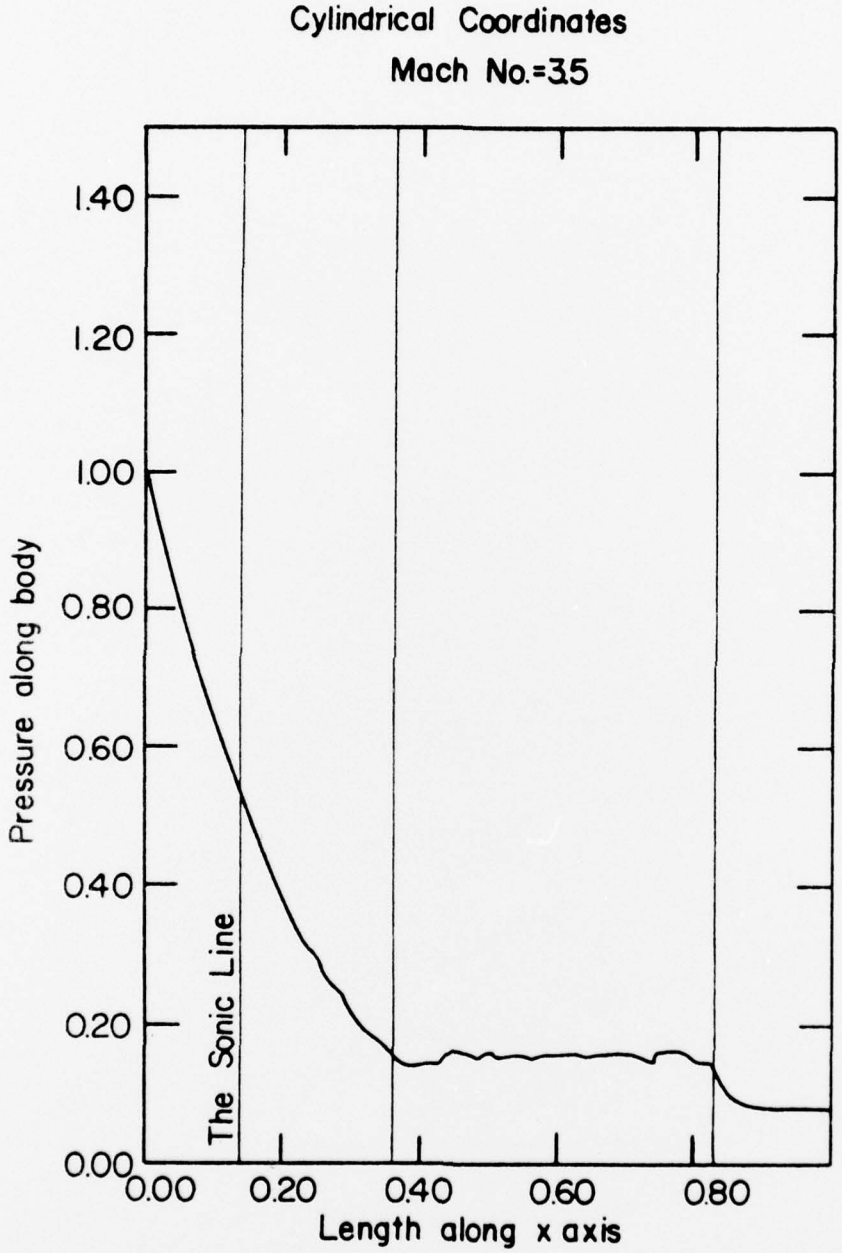
Cylindrical Coordinates
Mach No.=3.5
Pressure along body
1.40
1.20
1.00
0.80
0.60
0.40
0.20
0.00
The Sonic Line
0.00
0.20
0.40
0.60
0.80
Length along x axis

Fig. 15

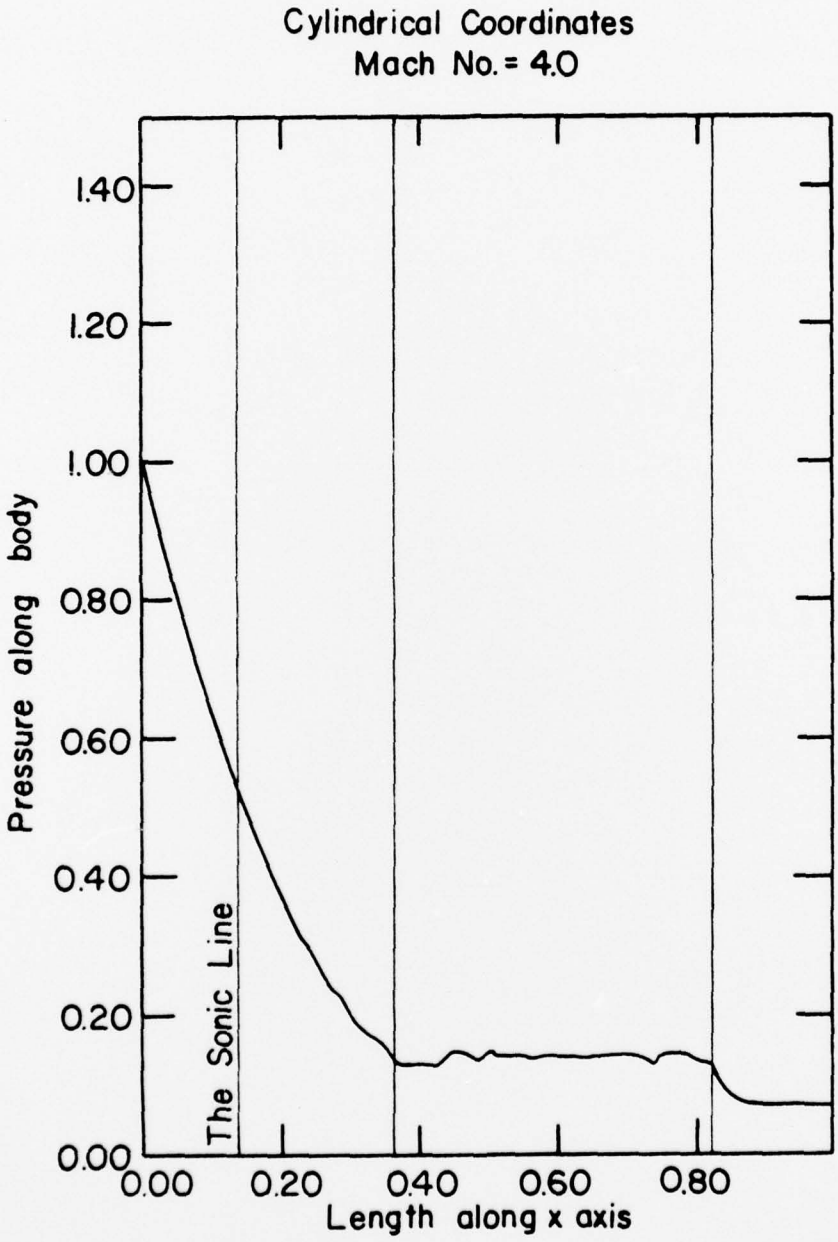
Cylindrical Coordinates
Mach No. = 4.0
Pressure along body
1.40
1.20
1.00
0.80
0.60
0.40
0.20
0.00
The Sonic Line
0.00
0.20
0.40
0.60
0.80
Length along x axis

Fig. 16

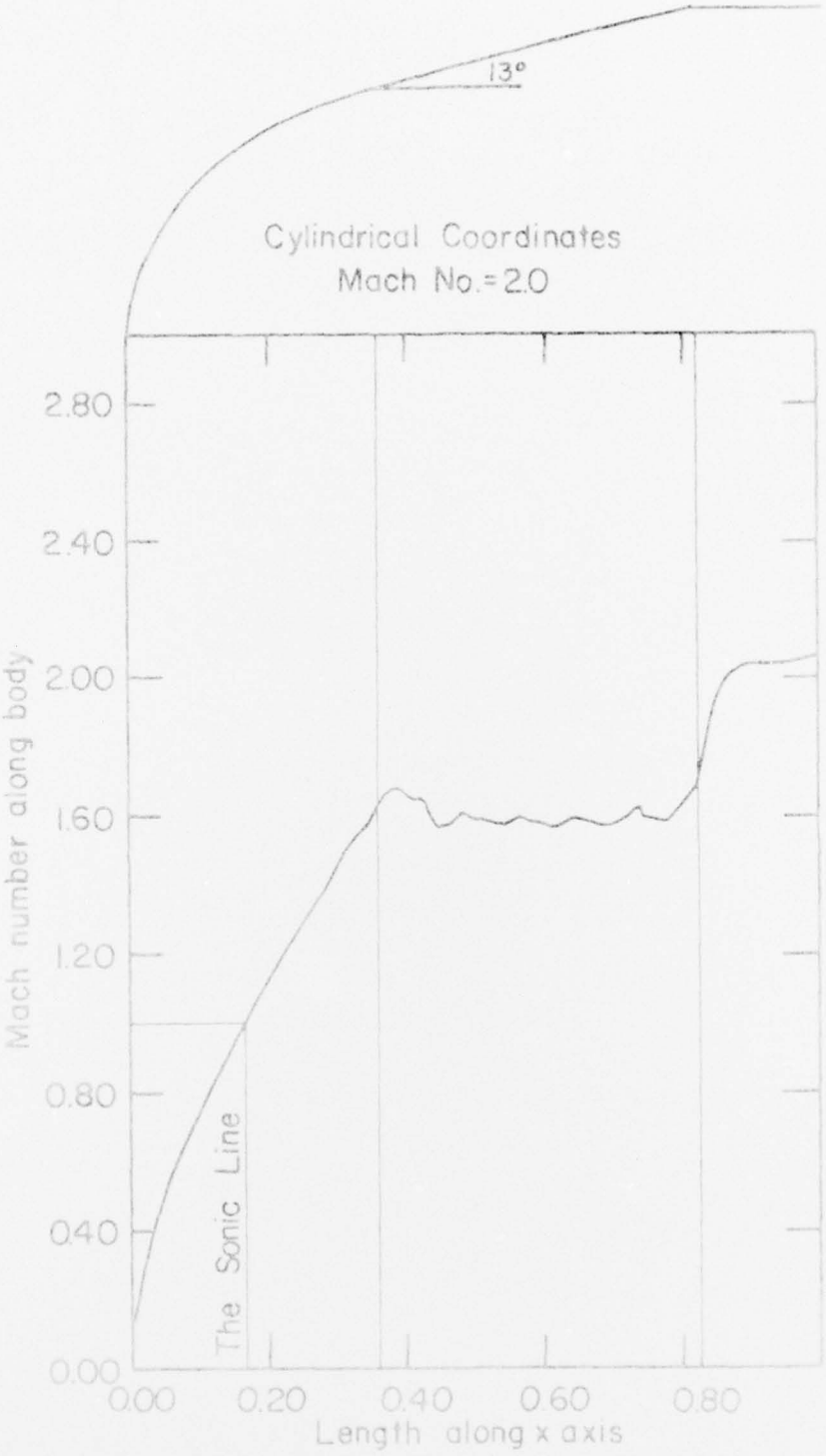
13°
Cylindrical Coordinates
Mach No.=2.0
2.80
2.40
2.00
1.60
1.20
0.80
0.40
0.00
Mach number along body
The Sonic Line
0.00
0.20
0.40
0.60
0.80
Length along x axis

Fig. 17

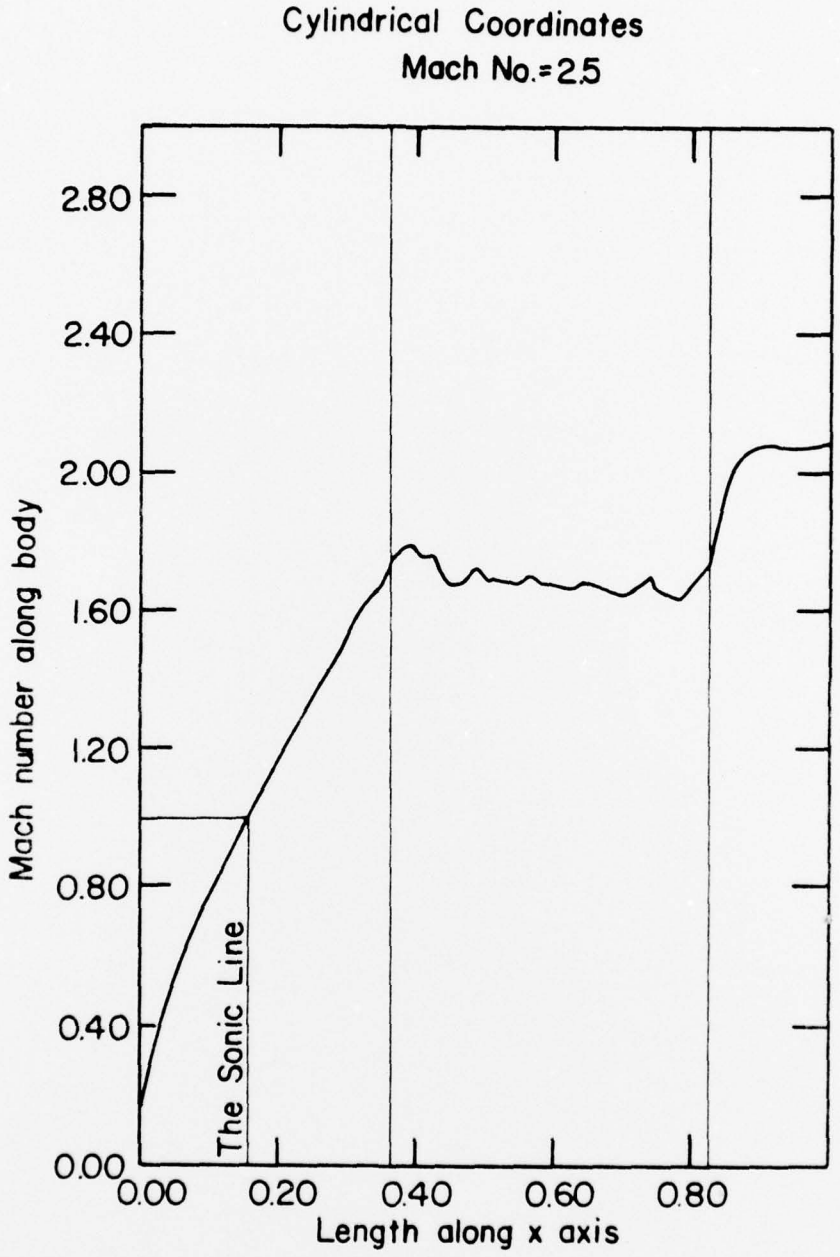
Cylindrical Coordinates
Mach No.=2.5
Mach number along body
2.80
2.40
2.00
1.60
1.20
0.80
0.40
0.00
The Sonic Line
0.00
0.20
0.40
0.60
0.80
Length along x axis

Fig. 18

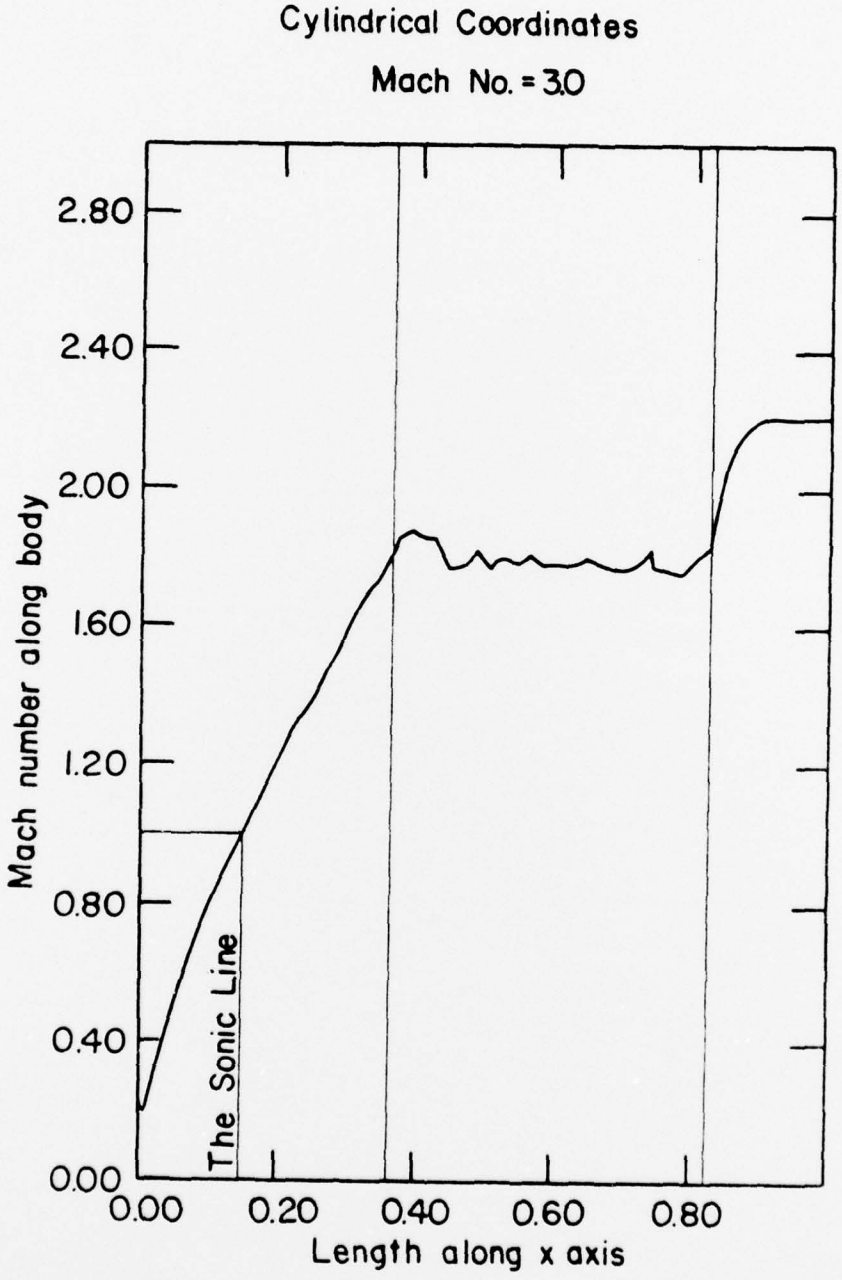
Cylindrical Coordinates
Mach No. = 3.0
Mach number along body
2.80
2.40
2.00
1.60
1.20
0.80
0.40
0.00
The Sonic Line
0.00
0.20
0.40
0.60
0.80
Length along x axis

Fig. 19

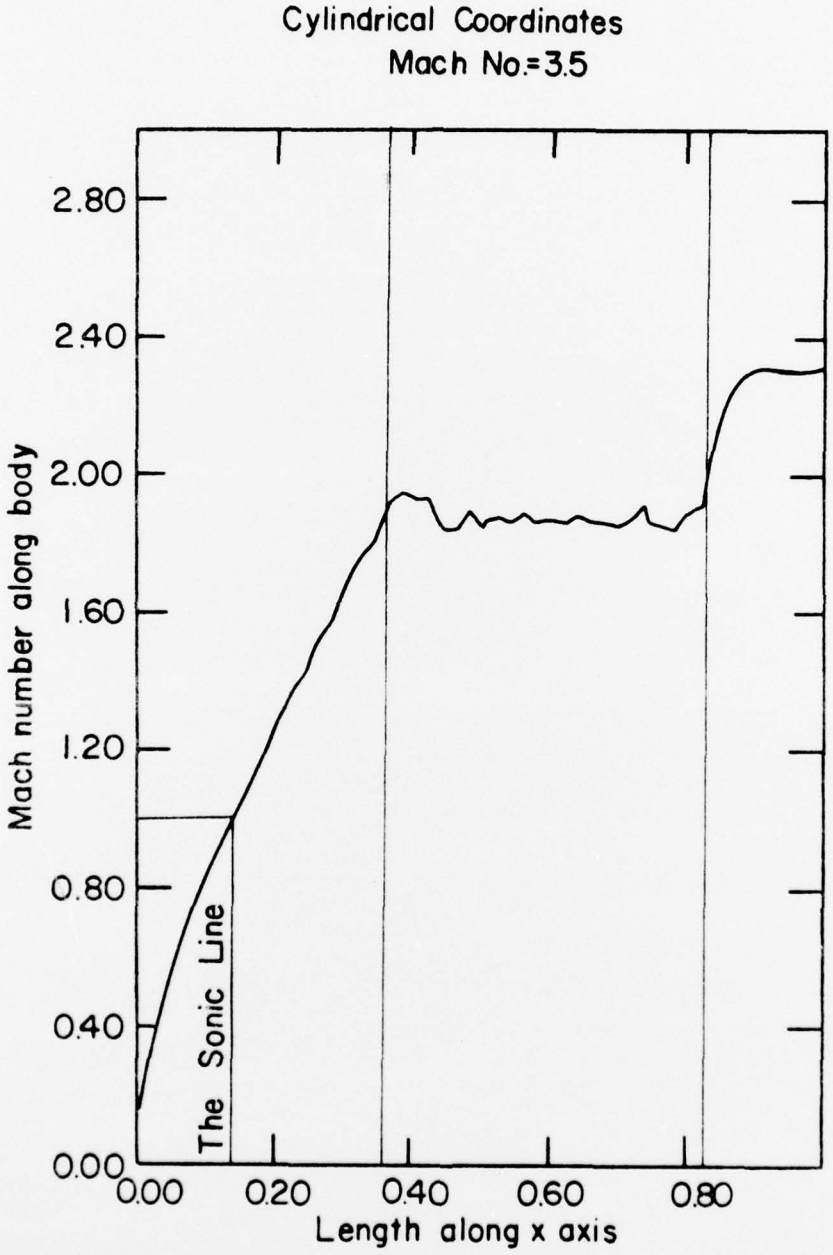
Cylindrical Coordinates
Mach No.=3.5
Mach number along body
2.80
2.40
2.00
1.60
1.20
0.80
0.40
0.00
The Sonic Line
0.00
0.20
0.40
0.60
0.80
Length along x axis

Fig. 20

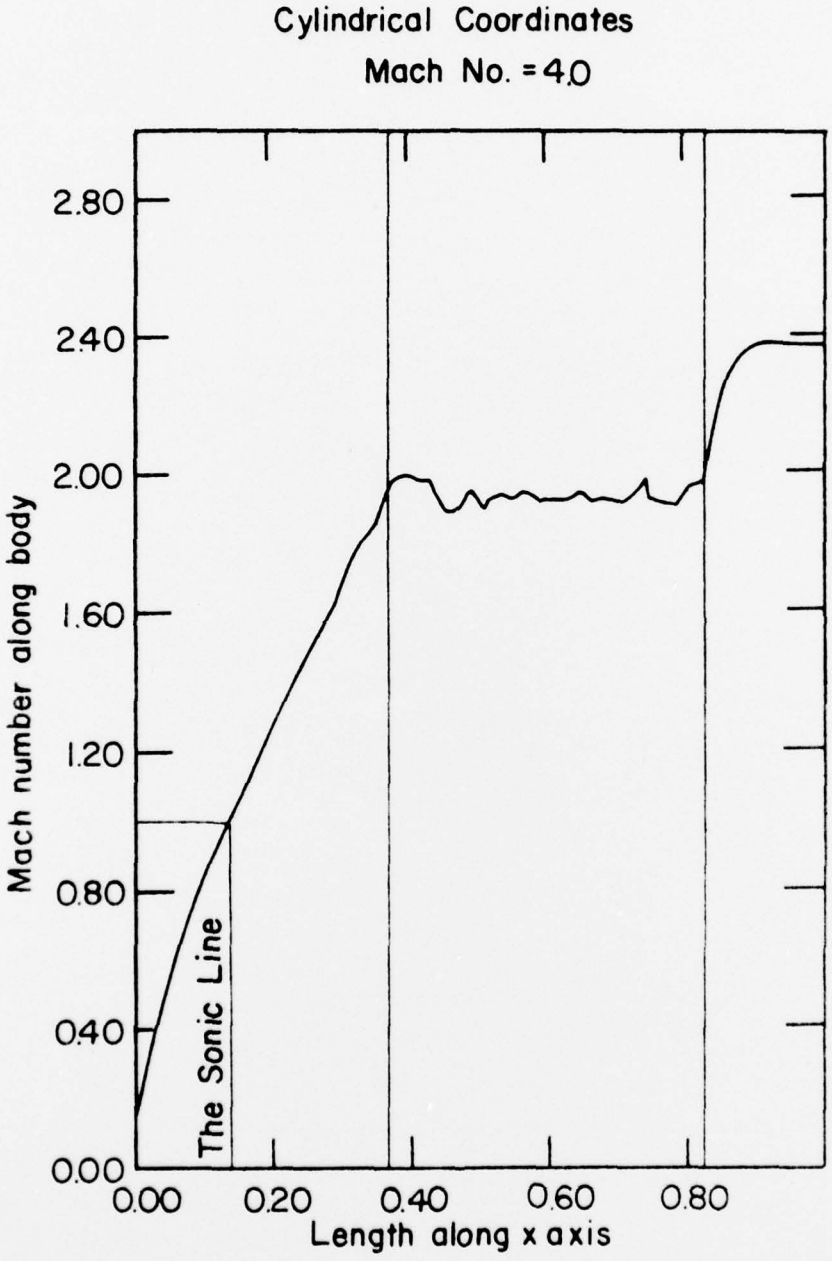
Cylindrical Coordinates
Mach No. = 4.0
Mach number along body
2.80
2.40
2.00
1.60
1.20
0.80
0.40
0.00
The Sonic Line
0.00
0.20
0.40
0.60
0.80
Length along x axis

Fig. 21

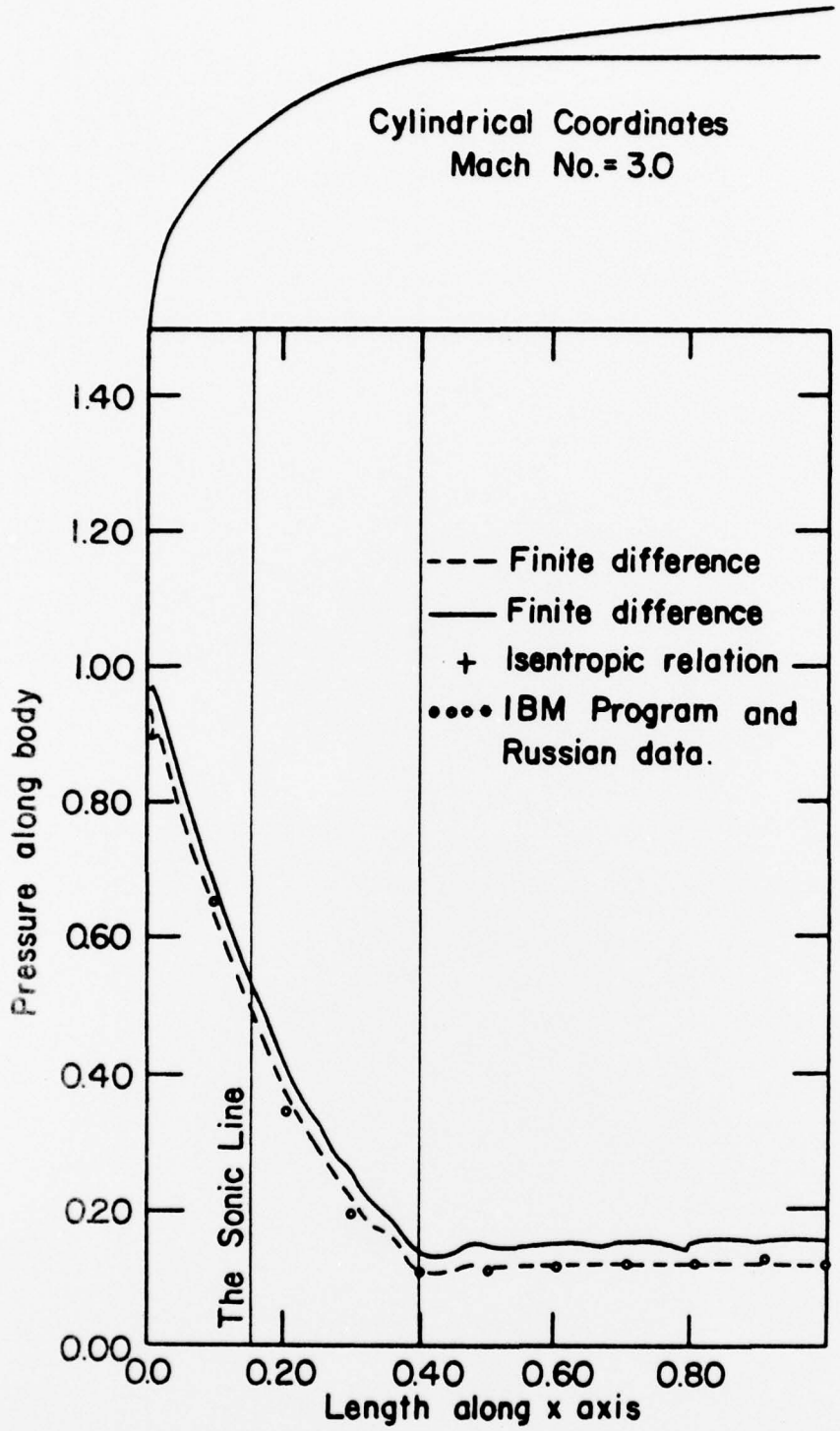

Fig. 22 COMPARISON OF THE PRESSURE DISTRIBUTION ALONG A BLUNTED CONE AS COMPUTED BY FINITE-DIFFERENCE METHOD (DASHED CURVE) WITH SEMI-EMPIRICAL FORMULA (OPEN CIRCLES).

$M_\infty = 3$, SEMI-APEX ANGLE = 10°

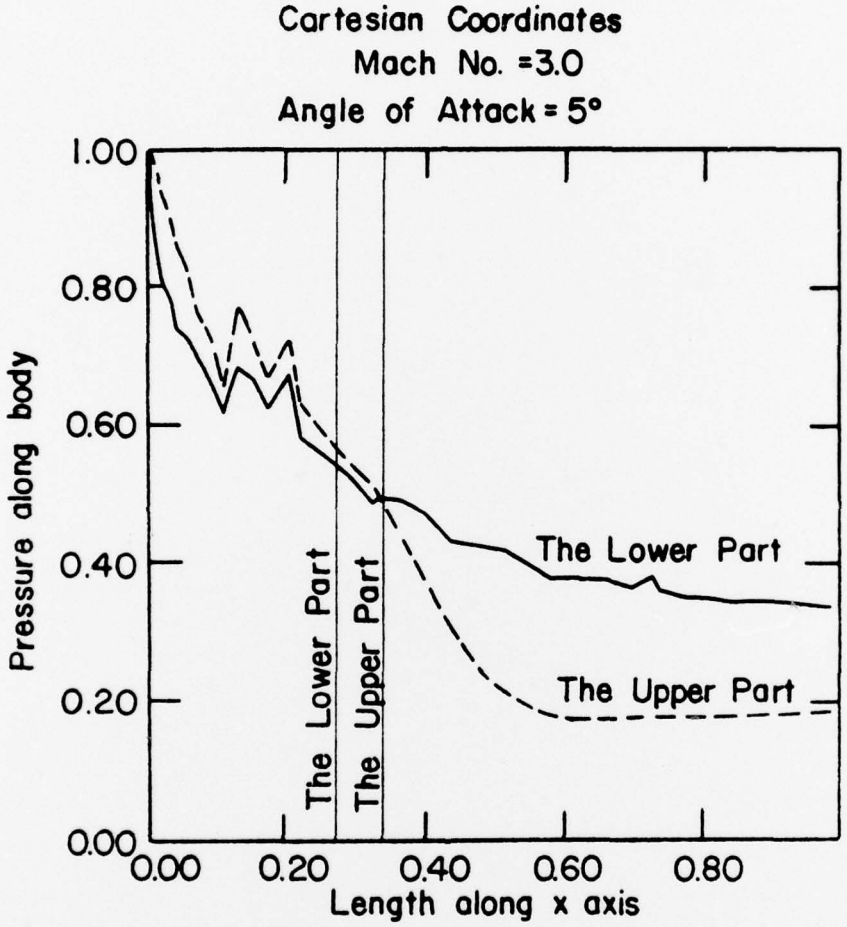
Cartesian Coordinates
Mach No. =3.0
Angle of Attack = 5°
1.00
0.80
0.60
0.40
0.20
0.00
Pressure along body
The Lower Part
The Upper Part
The Lower Part
The Upper Part
0.00
0.20
0.40
0.60
0.80
Length along x axis

Fig. 23a

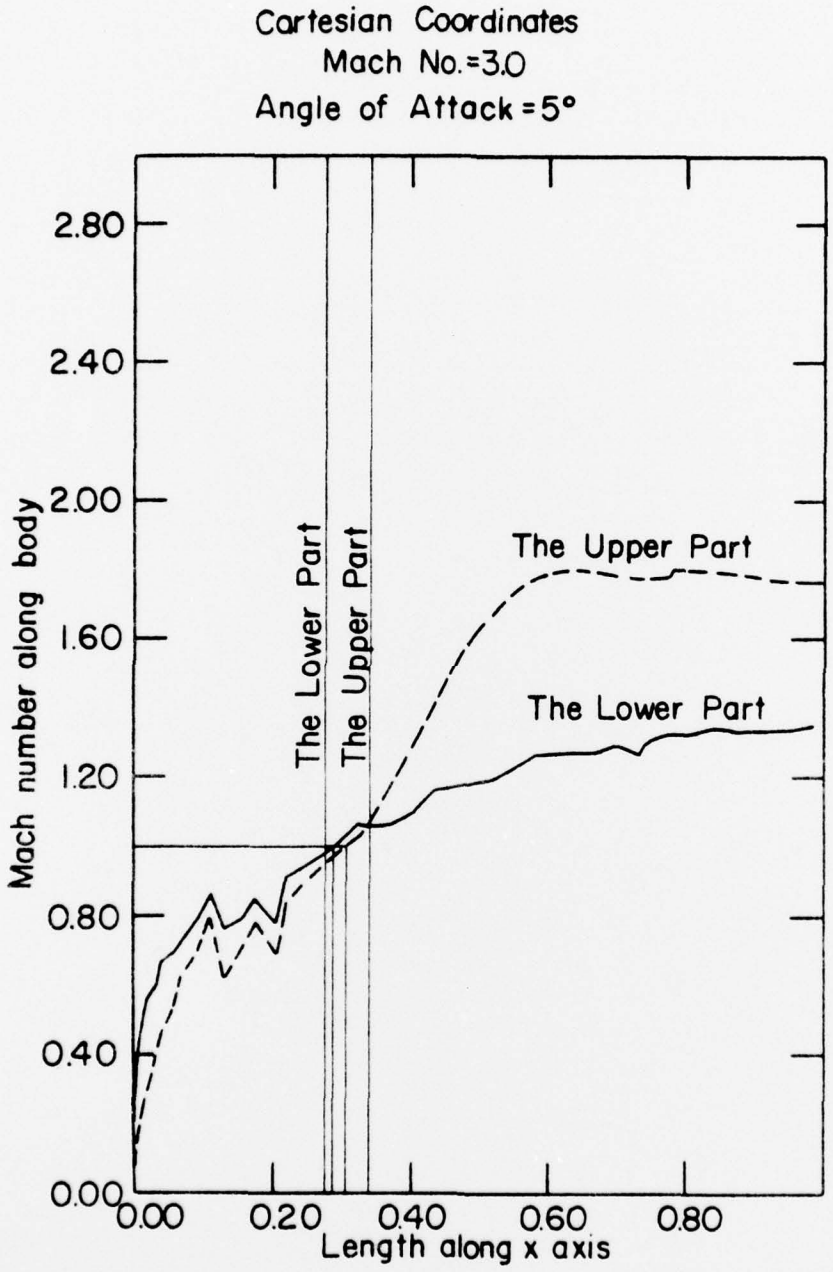
Cartesian Coordinates
Mach No.=3.0
Angle of Attack=5°
2.80
2.40
2.00
1.60
1.20
0.80
0.40
0.00
Mach number along body
The Lower Part
The Upper Part
The Upper Part
The Lower Part
0.00
0.20
0.40
0.60
0.80
Length along x axis

Fig. 23b

UNCLASSIFIED

SECURITY CLASSIFICATION OF THIS PAGE (When Data Entered)

REPORT DOCUMENTATION PAGE

READ INSTRUCTIONS BEFORE COMPLETING FORM

1. REPORT NUMBER: AFOSR - TR - 77 - 0162	2. GOVT ACCESSION NO.
3. RECIPIENT'S CATALOG NUMBER	
4. TITLE (and Subtitle): THE NUMERICAL COMPUTATIONS OF SUPERSONIC FLOW PAST BLUNT BODIES,	5. TYPE OF REPORT & PERIOD COVERED: INTERIM rept.
	6. PERFORMING ORG. REPORT NUMBER
7. AUTHOR(s): SAUL S. ABARBANEL	8. CONTRACT OR GRANT NUMBER(s): AFOSR 72-2370
9. PERFORMING ORGANIZATION NAME AND ADDRESS: TEL AVIV UNIVERSITY, DEPARTMENT OF MATHEMATICAL SCIENCES, RAMAT AVIV, ISRAEL	10. PROGRAM ELEMENT, PROJECT, TASK AREA & WORK UNIT NUMBERS: 9781-01, 61102F
11. CONTROLLING OFFICE NAME AND ADDRESS: AIR FORCE OFFICE OF SCIENTIFIC RESEARCH/NA, BLDG 410, BOLLING AIR FORCE BASE, D C 20332	12. REPORT DATE: 1976
	13. NUMBER OF PAGES: 49
14. MONITORING AGENCY NAME & ADDRESS (if different from Controlling Office): AF-AFOSR-2370-72	15. SECURITY CLASS. (of this report): UNCLASSIFIED
	15a. DECLASSIFICATION/DOWNGRADING SCHEDULE

16. DISTRIBUTION STATEMENT (of this Report)

9781 01

Approved for public release; distribution unlimited.

17. DISTRIBUTION STATEMENT (of the abstract entered in Block 20, if different from Report)

18. SUPPLEMENTARY NOTES

19. KEY WORDS (Continue on reverse side if necessary and identify by block number)

NUMERICAL METHODS
FINITE DIFFERENCE SCHEMES
SUPERSONIC FLOWS
BLUNT BODIES

20. ABSTRACT (Continue on reverse side if necessary and identify by block number)

Methods for computing numerically the flow past blunted bodies travelling at supersonic speed are developed, using finite difference schemes. The algorithms were constructed to deal with 2-D axisymmetric and 3-D configurations. Various configurations were investigated and the flow field around them computed. Comparison with available semi-empirical results for blunted cones at Mach number 3 shows good agreement. The 3-D algorithm was applied to an axisymmetric configuration and the results thus obtained show good agreement with the axisymmetric calculation. All the calculations are for the inviscid gas-dynamic case.

DD FORM 1 JAN 73 1473 EDITION OF 1 NOV 65 IS OBSOLETE

UNCLASSIFIED 706412

SECURITY CLASSIFICATION OF THIS PAGE (When Data Entered)